2015

Ferrite loaded coils for improved wireless power transfer efficiency

Rosenberry, Seth J.

Monterey, California: Naval Postgraduate School

NAVAL POSTGRADUATE SCHOOL

MONTEREY, CALIFORNIA

THESIS

FERRITE LOADED COILS FOR IMPROVED WIRELESS POWER TRANSFER EFFICIENCY

by

Seth J. Rosenberry

September 2015

Thesis Advisor: David Jenn
Second Reader: Roberto Cristi

Approved for public release; distribution is unlimited

THIS PAGE INTENTIONALLY LEFT BLANK

REPORT DOCUMENTATION PAGE	*Form Approved OMB No. 0704-0188*

1. AGENCY USE ONLY *(Leave blank)*	**2. REPORT DATE** September 2015	**3. REPORT TYPE AND DATES COVERED** Master's thesis

4. TITLE AND SUBTITLE
FERRITE LOADED COILS FOR IMPROVED WIRELESS POWER TRANSFER EFFICIENCY

5. FUNDING NUMBERS

6. AUTHOR(S) Rosenberry, Seth J.

7. PERFORMING ORGANIZATION NAME(S) AND ADDRESS(ES)
Naval Postgraduate School
Monterey, CA 93943-5000

8. PERFORMING ORGANIZATION REPORT NUMBER

9. SPONSORING /MONITORING AGENCY NAME(S) AND ADDRESS(ES)
N/A

10. SPONSORING / MONITORING AGENCY REPORT NUMBER

11. SUPPLEMENTARY NOTES The views expressed in this thesis are those of the author and do not reflect the official policy or position of the Department of Defense or the U.S. Government. IRB Protocol number ____N/A____.

12a. DISTRIBUTION / AVAILABILITY STATEMENT
Approved for public release; distribution is unlimited

12b. DISTRIBUTION CODE

13. ABSTRACT (maximum 200 words)

Recharging the battery system on Navy Autonomous Underwater Vehicles requires physical electrical contact between the vehicle and a docking station specifically designed to accommodate only one particular hull size. Inductive power transfer using mutually coupled coils eliminates physical contact, which can lead to an electrical short in a seawater environment, and provides the flexibility needed to create a docking station that can accommodate numerous hull sizes. Unfortunately, the power-transfer efficiency between these coils in an undersea environment can be very poor due to the conductivity of seawater.

To improve the power-transfer efficiency, the magnetic flux generated by the transmitting coil can be better concentrated through the receiving coil by careful geometric placement of ferrite materials. In this report, various ferrite configurations were evaluated using Computer Simulation Technology, and several high performance models were selected for construction and laboratory testing. The measured data collected in the laboratory are in good agreement with the simulation results, which indicate that the laboratory model and circuit closely adhered to the physical and electrical parameters of the simulation. This also underscores CST's usefulness for continued work in the field.

14. SUBJECT TERMS Wireless power transfer, inductive power transfer, autonomous underwater vehicle, mutually coupled coils, ferrite	**15. NUMBER OF PAGES** 77
	16. PRICE CODE

17. SECURITY CLASSIFICATION OF REPORT	**18. SECURITY CLASSIFICATION OF THIS PAGE**	**19. SECURITY CLASSIFICATION OF ABSTRACT**	**20. LIMITATION OF ABSTRACT**
Unclassified	Unclassified	Unclassified	UU

NSN 7540-01-280-5500 Standard Form 298 (Rev. 2-89)
Prescribed by ANSI Std. 239-18

THIS PAGE INTENTIONALLY LEFT BLANK

Approved for public release; distribution is unlimited

FERRITE LOADED COILS FOR IMPROVED WIRELESS POWER TRANSFER EFFICIENCY

Seth J. Rosenberry
Lieutenant Commander, United States Navy
B.S., United States Naval Academy, 2004

Submitted in partial fulfillment of the
requirements for the degree of

MASTER OF SCIENCE IN ELECTRICAL ENGINEERING

from the

NAVAL POSTGRADUATE SCHOOL
September 2015

Approved by: David Jenn
Thesis Advisor

Roberto Cristi
Second Reader

R. Clark Robertson
Chair, Department of Electrical and Computer Engineering

THIS PAGE INTENTIONALLY LEFT BLANK

ABSTRACT

Recharging the battery system on Navy Autonomous Underwater Vehicles requires physical electrical contact between the vehicle and a docking station specifically designed to accommodate only one particular hull size. Inductive power transfer using mutually coupled coils eliminates physical contact, which can lead to an electrical short in a seawater environment, and provides the flexibility needed to create a docking station that can accommodate numerous hull sizes. Unfortunately, the power-transfer efficiency between these coils in an undersea environment can be very poor due to the conductivity of seawater.

To improve the power-transfer efficiency, the magnetic flux generated by the transmitting coil can be better concentrated through the receiving coil by careful geometric placement of ferrite materials. In this report, various ferrite configurations were evaluated using Computer Simulation Technology, and several high performance models were selected for construction and laboratory testing. The measured data collected in the laboratory are in good agreement with the simulation results, which indicate that the laboratory model and circuit closely adhered to the physical and electrical parameters of the simulation. This also underscores CST's usefulness for continued work in the field.

THIS PAGE INTENTIONALLY LEFT BLANK

TABLE OF CONTENTS

I. INTRODUCTION....1
A. AUTONOMOUS UNDERWATER VEHICLES....1
B. WIRELESS POWER: THE WAY FORWARD....1
C. OTHER WORK....4
D. OBJECTIVE....5
E. THESIS ORGANIZATION....6

II. THEORY....7
A. INDUCTIVE POWER TRANSFER....7
B. MUTUALLY COUPLED COILS....7
C. RESONANT INDUCTIVE COUPLING....9
D. IMPEDANCE MATCHING....10
E. FERRITE MATERIAL....12

III. CST SIMULATIONS....15
A. MODEL DESIGN....15
B. SEPARATION DISTANCE CONSIDERATIONS....17
C. SIMULATION RESULTS....19
D. LATERAL MISALIGNMENT TESTING....28
E. SENSITIVITY ANALYSIS....30
F. SEAWATER SIMULATION....32

IV. LABORATORY TESTING....35
A. SYSTEM SETUP....35
B. MEASURING POWER TRANSFER EFFICIENCY....39
C. COMPARISON OF SIMULATED AND MEASURED RESULTS....43

V. SUMMARY, CONCLUSIONS, AND FUTURE WORK....45
A. SUMMARY....45
B. CONCLUSIONS....45
C. FUTURE WORK....47

APPENDIX A. MATLAB SCRIPT FILE: RESISTIVE LOADS....49

APPENDIX B. MATLAB SCRIPT FILE: CAPACITANCE....53

LIST OF REFERENCES **57**

INITIAL DISTRIBUTION LIST **59**

LIST OF FIGURES

Figure 1. REMUS approaching an underwater docking station designed specifically for its hull size, from [2]. 2

Figure 2. Basic WPT concept diagram. 3

Figure 3. The mooring profiler ITP system. The insertion core can be seen in the lower left-hand corner, and the guidance cable is visible in yellow, from [4]. 4

Figure 4. The Odyssey AUV conducting research operations, from [6]. 5

Figure 5. Example of a mutually coupled core model generated using Computer Simulation Technology (CST). 6

Figure 6. A magnetic flux in Coil 2 is produced when current is applied to Coil 1, from [9]. 8

Figure 7. The magnetic flux generated in Coil 2 causes current I_2 to flow, from [9]. 8

Figure 8. A series-series compensated circuit showing the placement of the components used for assembly and testing, from [1]. 10

Figure 9. A two-coil model for simulation. The color blue represents vacuum, green is ferrite, and red is seawater. The circuit component colors have no significance. 16

Figure 10. Example of a polar plot showing impedance values for a range of resistive loads. 17

Figure 11. Distance between transmitting and receiving coils, coil mounting system used in prior research, and the zip ties that limit minimum separation distance, from [1]. 18

Figure 12. New coil mounting system which minimizes coil spacing. 18

Figure 13. A CST model showing two mutually coupled coils in a vacuum. 19

Figure 14. CST model showing ferrite back plates and a coil separation of 16.0 mm. 20

Figure 15. Efficiency comparison of CO and CP models. 21

Figure 16. CST model with solid ferrite cores and ferrite back plates. 22

Figure 17. Efficiency comparison of CP and CCP models. 23

Figure 18. Efficiency comparison of the CCP model (μ_r = 220) with and without capacitance. 25

Figure 19. CST model showing hollow ferrite cores with wall thickness of 3.0 mm and ferrite back plates. 26

Figure 20. Comparison of CCP model (μ_r = 220) with the HCP model (μ_r = 220). 27
Figure 21. CST model showing hollow ferrite cores and back plates with a thickness of 0.1 mm. 28
Figure 22. CCP model misaligned 10.0 mm. 29
Figure 23. The CCP model is shown with a thin cylinder of seawater filling the 16.0 mm gap between the coils. 32
Figure 24. Efficiency comparison of optimum model and coils only model at 16.0 mm in seawater. 33
Figure 25. Block diagram showing components of laboratory test circuit. 35
Figure 26. Laboratory setup displaying circuit components, power supply, and monitoring equipment. 36
Figure 27. One of two 15.0 pF capacitors used to achieve optimum circuit performance. 37
Figure 28. Transmitting coil mounted on vertical wooden stand and base. 38
Figure 29. Test coil mounted on vertical wooden stand (without ferrite). 38
Figure 30. Test coil shown with ferrite back plate. 40
Figure 31. Test coil shown with ferrite back plate and ferrite-covered plastic cylinder. 40
Figure 32. Efficiency of laboratory models for various coil separations. 42
Figure 33. Reshaped ferrite back plate and test coil. 43
Figure 34. Test coil shown inside cross-section of aluminum representing REMUS hull, from [1]. 47
Figure 35. System mockup of AUV in docking/charging station. 48

LIST OF TABLES

Table 1. Laboratory coil physical and electrical properties, from [1].....16

Table 2. CST results for the reference model shown in Figure 13. 20

Table 3. CST results for the model shown in Figure 14. 21

Table 4. CST results for the model shown in Figure 16. 22

Table 5. CST results for model constructed with ferrite cores and back plates with relative permeability of 220. 24

Table 6. CST results for the CCP model (μ_r = 220) with a compensating capacitance of 13.5 pF. 24

Table 7. CST results for model shown in Figure 19. 26

Table 8. CST results for model shown in Figure 21. 28

Table 9. Results for CCP model misaligned 5.0 mm. 29

Table 10. Results for CCP model misaligned 10.0 mm. 30

Table 11. Sensitivity analysis showing percent reduction in power-transfer efficiency from a 16.0 mm coil separation gap to a 32.0 mm gap for the CO model. 31

Table 12. Sensitivity analysis showing percent reduction in power-transfer efficiency from a 16.0 mm coil separation gap to a 32.0 mm gap for the CCP model. 31

Table 13. Comparison of the efficiency reduction for a 16.0 mm coil separation distance when the CO model and the CCP model are moved from a vacuum to seawater. 33

Table 14. Efficiency results for round 1 (coils only). 41

Table 15. Efficiency results for round 2 (with ferrite back plates). 41

Table 16. Efficiency results for round 3 (with ferrite back plates and hollow cores). 41

Table 17. Lateral separation efficiency for coils with ferrite back plates and cores at 16.0 mm. 42

Table 18. Lateral separation efficiency for coils with ferrite back plates and cores at 32.0 mm. 42

THIS PAGE INTENTIONALLY LEFT BLANK

LIST OF ACRONYMS AND ABBREVIATIONS

AUV	Autonomous Underwater Vehicle
CST	Computer Simulation Technology AG
EMF	Electromotive Force
IPT	Inductive Power Transfer
MWS	Microwave Studio
NEC	Numerical Electromagnetics Code
REMUS	Remote Environmental Measuring Units
UAV	Unmanned Aerial Vehicle
WHOI	Woods Hole Oceanographic Institute
WPT	Wireless Power Transfer

THIS PAGE INTENTIONALLY LEFT BLANK

ACKNOWLEDGMENTS

I would like to thank the following people for their help during this thesis work. Your advice, support and guidance mean a lot to me and were critical in the successful completion of this work.

David Jenn, Naval Postgraduate School
Roberto Cristi, Naval Postgraduate School
Robert Broadston, Naval Postgraduate School
My family: Boyden, Debbie, Jason, Ana, Forest, and Naomi

THIS PAGE INTENTIONALLY LEFT BLANK

I. INTRODUCTION

A. AUTONOMOUS UNDERWATER VEHICLES

Autonomous underwater vehicles (AUVs) are generally lightweight, unmanned robotic machines capable of performing a wide variety of tasks including scientific research, environmental monitoring, underwater mapping, and military-related assignments. Complimented by highly sophisticated software systems, AUVs benefit from the ability to complete relatively complex assignments without operator input. Additionally, AUVs utilize internal power supplies, usually rechargeable batteries, which allow for untethered operations far from their point of insertion. It is the way the batteries are charged, however, which limits the full potential of these vehicles. The majority of AUVs with rechargeable batteries must return to their respective power sources, whether this is a surface vessel or a charging dock, and then an operator must connect a power cable. For AUVs conducting environmental monitoring operations, for example, continuous return trips to a common power source is costly from a time-management perspective. AUVs with an accompanying surface vessel acting as a mother ship can greatly reduce this cost while simultaneously increasing the effective area in which the AUV operates, but it is costly to keep a vessel at sea. In essence, AUVs are not entirely autonomous and are in need of an entirely new charging system to complement their high-end capabilities.

B. WIRELESS POWER: THE WAY FORWARD

Wireless power transfer (WPT) offers a solution to the problems associated with tethered charging. With a set of mutually coupled coils separated by a seawater gap, AUVs could recharge their batteries by means of inductive power transfer (IPT). IPT allows for the wireless transfer of energy between two separate coils of wire by means of a linked magnetic flux. With the state-of-the-art navigation systems already in use on some AUVs, recharging onboard batteries would be as simple as navigating to the closest underwater charging station, conducting a charge, and returning to normal

operations. Since an operator is not required, charging stations could be placed almost anywhere.

In 2013, a study was conducted at the Naval Postgraduate School in which pairs of mutually coupled coils were extensively tested in order to provide the framework for a suitable replacement for the charging system currently employed on the Navy's Remote Environmental Measuring Units (REMUS) AUV (see Figure 1) [1]. IPT using mutually coupled coils was proposed as an alternative to the charging system in use. The research was motivated by the shortfalls in the REMUS charging station; specifically, the charging station was designed to accommodate only one particular hull size and, additionally, exposure to seawater poses the risk of electrically shorting the AUV should the electrical contacts corrode. By wirelessly transferring power through a seawater gap, a charging system can be developed to accommodate AUVs of varying sizes and prevent physical contact, thereby eliminating the possibility of shorting the AUV.

Figure 1. REMUS approaching an underwater docking station designed specifically for its hull size, from [2].

The basic WPT concept is illustrated in Figure 2. It consists of a base station which provides power to the transmitting coil. On the client side, received power is conditioned and then delivered to the battery charger or power plant.

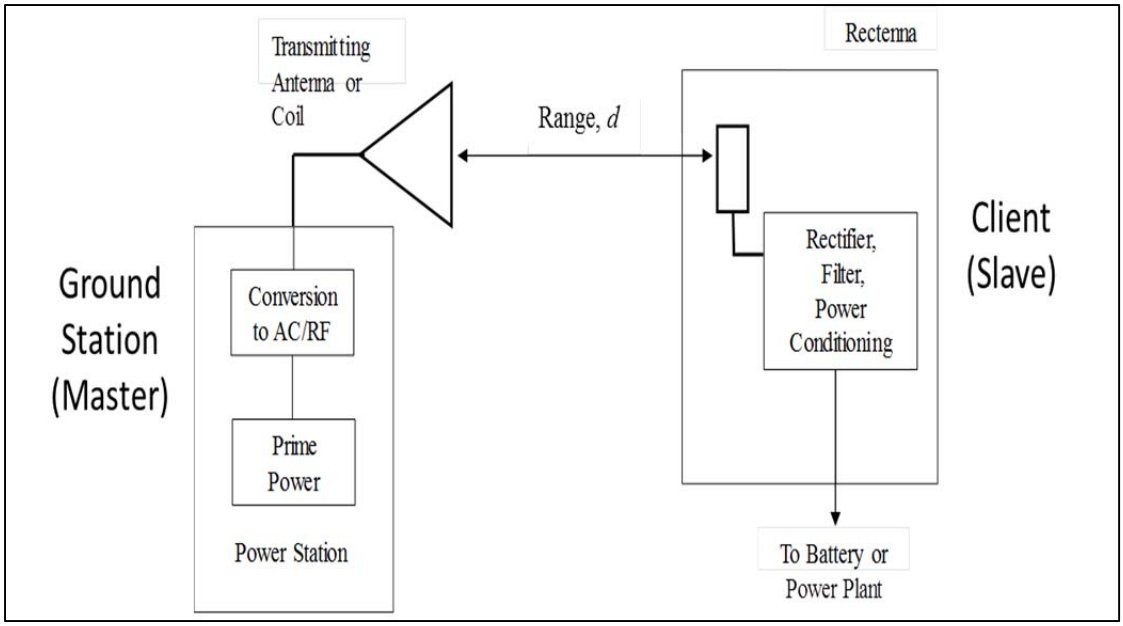

Figure 2. Basic WPT concept diagram.

While inductive power transfer is a proven technology in some commercial applications, such as charging electronic toothbrushes and cellphones, there are several problems inherent to utilizing this method with an AUV in a seawater environment. In particular, earlier research indicated that increasing the operating frequency above 100 kHz causes an undesirable increase in resistance due to the conductivity of seawater [1], [3]. While operating frequency was shown to be limited for operations in a seawater environment, placing a few small sheets of ferrite behind the coils shows some improvement in overall power-transfer efficiency [1]. The ferrite used in laboratory tests for this analysis and the prior study is an iron-based material used to concentrate the magnetic flux generated by the transmitting coil toward the receiving coil. Based on these promising results [1], the task of identifying the optimum geometric configuration of ferrite materials placed in the vicinity of mutually coupled coils is addressed in this work. It is shown in Chapter III that the power-transfer efficiency of mutually coupled coils can be greatly improved by the careful geometric placement of ferrite materials in close proximity to the coils.

C. OTHER WORK

In the preceding section, some of the challenges of using ITP in a seawater environment were introduced. This has not deterred meaningful research and experimentation on the subject. In 2007, a study was conducted for a new underwater mooring profiler that was able to collect data from a seafloor observatory and transfer the information to a subsurface platform using ITP [4]. While the data transfer was occurring, the profiler was able to recharge its batteries via the same method. The profiler benefited from a guidance cable that allowed for the insertion of a magnetically permeable core between two separate coils (see Figure 3). The core provided a guide for the magnetic flux and improved overall power transfer efficiency. For REMUS, having an insertion core would greatly increase the complexity of the charging station, and it would be difficult to align the two-coil system without the introduction of a guidance cable.

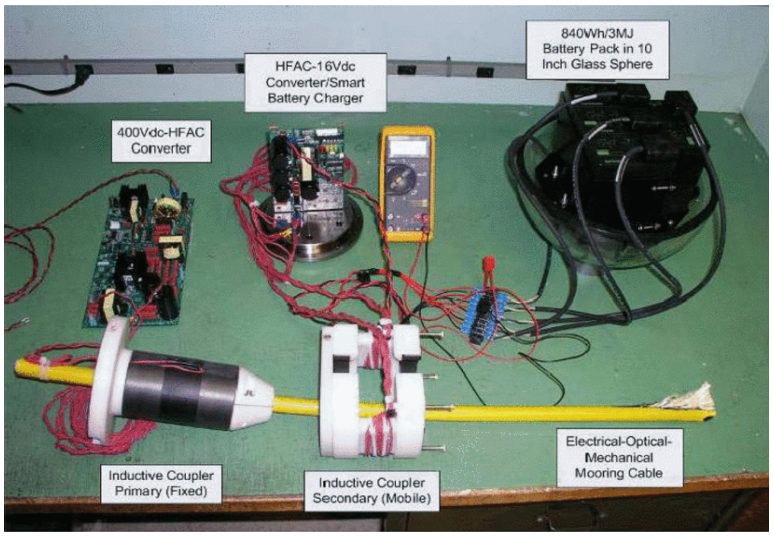

Figure 3. The mooring profiler ITP system. The insertion core can be seen in the lower left-hand corner, and the guidance cable is visible in yellow, from [4].

In May of 2005, a study at the Massachusetts Institute of Technology was conducted in which a new charging system for the Odyssey AUV was proposed [5]. Odyssey is a deep-diving AUV used for scientific research (see Figure 4). The design allowed for the insertion of a primary core between two secondary cores. Additionally,

the design benefitted by a gap of only 0.5 millimeters, which helped to increase its overall performance. As is discussed in Chapter III, the smallest gap used in this research was 16 millimeters.

Figure 4. The Odyssey AUV conducting research operations, from [6].

D. OBJECTIVE

The objective of this research was to determine the optimum mutually coupled coil model which could serve as the primary component of a replacement charging system for the Navy's AUVs. Using a computational electromagnetic model of a two-coil system generated with the commercial software package Microwave Studio, a product by Computer Simulation Technology AG (CST), we were able to demonstrate how changing various parameters of an IPT model affects its efficiency. An example of the CST model is shown in Figure 5. The parameters included the magnetic permeability of ferrite, the width of the gap between the transmitting and receiving coils, the dimensions of the ferrite sheets used, the compensating capacitance for the overall circuit, and lateral misalignment of the coils. In the next chapter, it is shown that adding a specific capacitance to the charging circuit allows system to achieve optimum efficiency. The goal was to determine which parameter set produced the highest efficiency while still considering the overall size, weight, and cost of the design. Several of the best performing models were selected and constructed for use in laboratory tests.

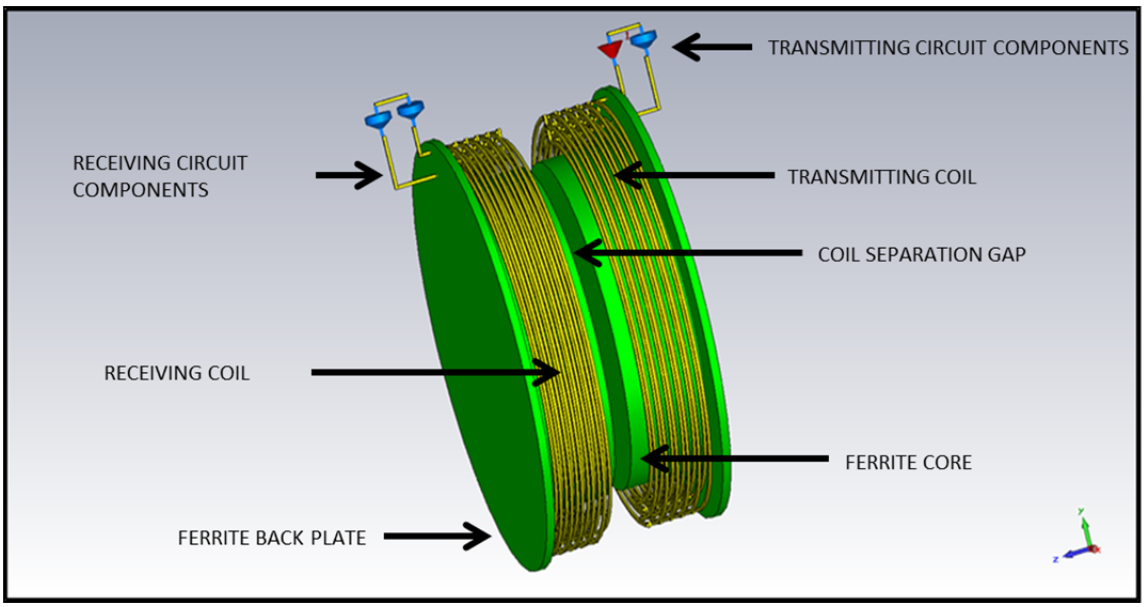

Figure 5. Example of a mutually coupled core model generated using Computer Simulation Technology (CST).

E. THESIS ORGANIZATION

This thesis is organized into five chapters. In Chapter I, prior research was mentioned along with its accompanying issues and potential solutions. Ferrite material is introduced as the primary focus for improving the efficiency of a replacement charging system for AUVs. In Chapter II, the physics of IPT are briefly discussed in order to provide a basic understanding of mutually coupled coils. Capacitance and its relationship to an efficient power system are then dissected and, finally, ferrite and its highly desirable properties are discussed in detail. In Chapter III, we take an extensive look at the CST models and discuss the method that was employed during testing and analysis. Simulation results are also discussed, and a few of the configurations are selected for use in the laboratory testing. The results of Chapter III are built on in Chapter IV. Three specific models were selected and built in order to provide measured data that could be compared to the simulated data recorded from CST. Finally, the research in its entirety is summarized and new areas of research are selected in Chapter V, and areas are proposed for further review and analysis.

II. THEORY

A. INDUCTIVE POWER TRANSFER

Before the discussion of a two-coil charging system can begin, it is important to have a basic understanding of IPT. Faraday's Law states that a time-varying magnetic field can induce a voltage in a circuit [7]. It was not, however, widely accepted until James Maxwell was able to demonstrate mathematically that the rate of change of the magnetic field within a circuit was equal to the induced electromotive force (EMF). Heinrich Lenz further contributed to the idea by proving that an induced current always moves in a direction opposite to that of the force which created it [8]. As it came to be known, the Maxwell-Faraday equation is expressed as [9]

$$V = -N\frac{\partial \Phi}{\partial t}. \tag{1}$$

In Equation (1), V is the electromotive force, N is the number of turns in a coil of wire, and Φ is the magnetic flux.

B. MUTUALLY COUPLED COILS

Mutually coupled coils imply that there is inductance between two loops of wires. This means that a change in current in the transmitting coil induces a voltage in the receiving coil. In Figure 6, it can be observed that the magnetic field B_1 generated by a current I_1 produces magnetic flux that links Coil 2, which induces a current I_2. In Figure 7, some of the magnetic flux of Coil 2 due to current I_2 links Coil 1, inducing current I_1.

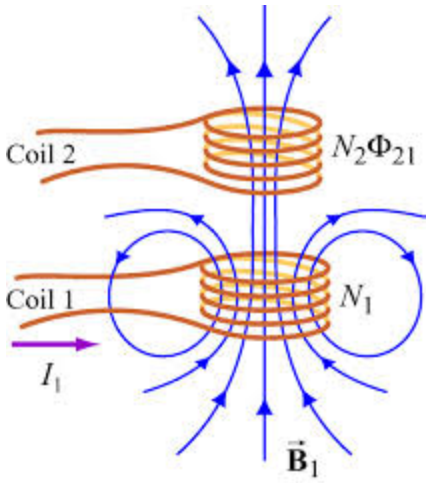

Figure 6. A magnetic flux in Coil 2 is produced when current is applied to Coil 1, from [9].

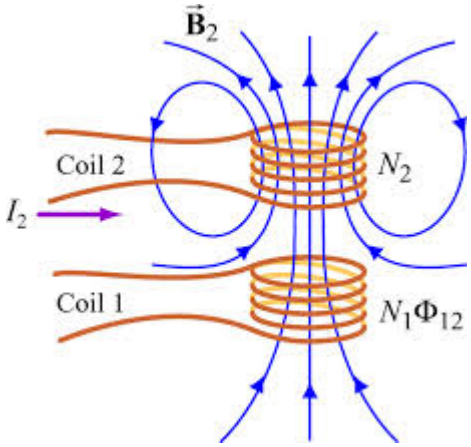

Figure 7. The magnetic flux generated in Coil 2 causes current I_2 to flow, from [9].

With reference to Figure 6, if the magnetic field B_1 is proportional to the current which produced it, then it is intuitive that the magnetic flux generated in Coil 2 by B_1 is also proportional to I_1. Mutual inductance M is the parameter used to describe this relationship and is important because it represents the degree to which two inductors are coupled [10]. Because of this, when a current is applied to either of the coils, independence is absent and there exists a mutual dependence of each coil on the other. The voltage generated at the output of Coil 2 due to current flow in Coil 1 is given by [9]

$$V_{21} = N_2 \frac{\partial \Phi_{21}}{dt} = M_{21} \frac{\partial I_1}{dt}. \quad (2)$$

In Equation (2), M_{21} is the mutual inductance that exists between the coils, N_2 is the number of turns of Coil 2, and Φ_{21} is the magnetic flux from Coil 1 to Coil 2.

C. RESONANT INDUCTIVE COUPLING

Mutual coupling between two inductors is classified as either loose or tight. This is somewhat arbitrary, with the former encompassing a much greater spectrum of systems and devices. A tightly coupled system is most easily explained by an ideal transformer. Like any transformer, this ideal device creates a magnetic flux within its magnetically permeable core via the primary winding, and an electromotive force is generated in the secondary winding. Unlike practical transformers, however, the ideal model is able to contain all of the magnetic flux within its core, there are no energy losses, and the magnetic permeability of the core is infinite [11]. Magnetic permeability is the measure of a material's ability to concentrate a magnetic field. Transformers in general are considered tightly coupled systems due to the existence of a highly permeable core, while most other systems, particularly those required for transmitting wireless power through a gap of any width, are said to be loosely coupled. Intuitively, this implies high energy losses and a magnetic flux that is partially unutilized. To combat these losses, loosely coupled inductors are designed to resonate at the same frequency as one another [12]. To achieve this, each inductor must employ a specific compensating capacitor that is mathematically related to the inductance of each coil.

For tests conducted for this study, all components for each coil were connected in a series configuration, better known as series-series compensation (see Figure 8). The term compensation stems from the use of compensating capacitors C_1 and C_2. The components included a voltage source V_S, compensating capacitors, the coils themselves, and a resistive load R_L. The resistors R_1 and R_2 are the internal resistances of the coils and L_1 and L_2 are the inductances. Compensating the circuit in this way was done primarily for simplicity and to maintain continuity with prior research [1].

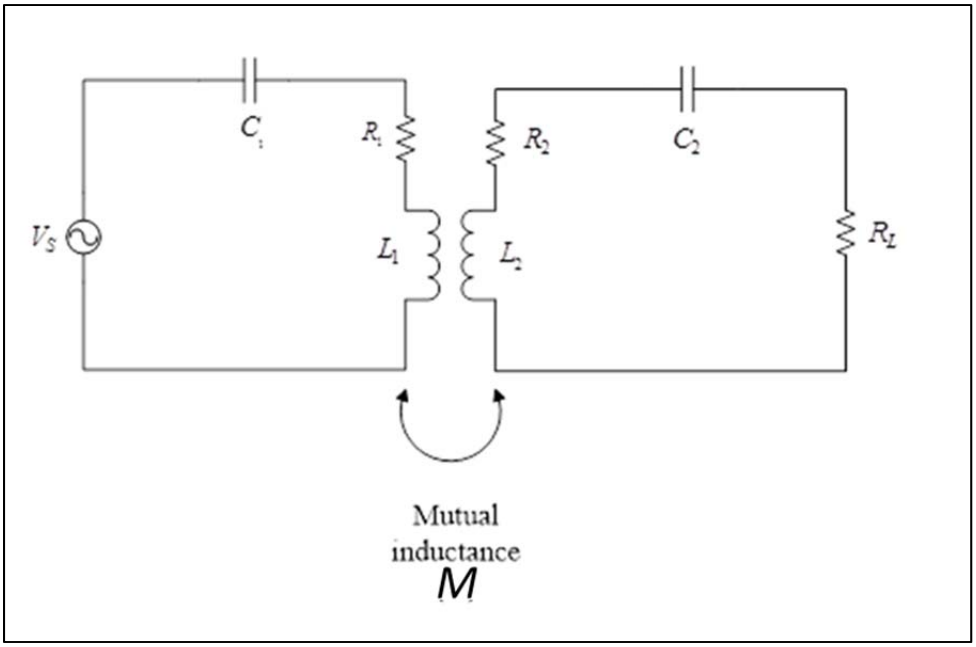

Figure 8. A series-series compensated circuit showing the placement of the components used for assembly and testing, from [1].

The compensating capacitance is determined using the angular frequency ω_0 of the circuit and the corresponding inductance of the coils. The relationship between inductance, angular frequency, and capacitance is

$$C = \frac{1}{L\omega_0^2}. \tag{3}$$

In this study the operating frequency-of-interest is 100 kHz. Using the inductance values of the coils determined in [1], we selected the appropriate capacitor for each coil.

D. IMPEDANCE MATCHING

With compensating capacitance determined, the final step required for a series-series compensated circuit to exhibit optimum performance is to match the impedance of the circuit. Impedance is a measure of an electrical circuit's opposition to the transfer of energy to a load, and impedance matching is required for maximum power transfer from the source to the load [13]. In the case of the circuit used in this study, maximum power transfer is achieved when the complex conjugate of the impedance of the power source Z^*_{source} is equated to the impedance of the load Z_{load}. This is expressed as

$$Z_{load} = Z^*_{source}. \tag{4}$$

In Equation (4), Z_{load} is the combined impedance of the circuit components on the load side, while Z^*_{source} is the combined impedance of the source components. With known values for the capacitors, coil resistances, and the voltage source, the remaining component of the circuit, R_L, must be determined in order to impedance match the circuit. The value of R_L is determined from the circuit efficiency calculation of the compensated series-series circuit in Figure 8 [1], [13]. The efficiency η is given by

$$\eta = \frac{R_L(\omega_0 M)^2}{R_1(R_2 + R_L)^2 + (\omega_0 M)^2(R_2 + R_L)}. \tag{5}$$

To determine the value of the load resistance, the derivative of Equation (5) is taken with respect to R_L. The resulting expression is then set equal to zero, yielding

$$\begin{aligned} 0 = {} & (\omega M)^2[R_1R_2^2 + 2R_1R_2R_L + (\omega M)^2 R_2 + (\omega M)^2 R_L]^{-1} \\ & -[R_1R_2^2 + 2R_1R_2R_L + R_1R_L^2 + (\omega M)R_2 + (\omega M)^2 R_L]^{-2}([R_L(\omega M)^2] \\ & [2R_1R_2 + 2R_1R_L + (\omega M)^2]). \end{aligned} \tag{6}$$

Next, Equation (6) is simplified and solved for R_L. Since a resistive load is necessary to match the impedance of the circuit, R_L is now referred to as $R_{L,matched}$ [1], [14] and is expressed as

$$R_{L,matched} = \sqrt{R_2^2 + (\omega M)^2 \frac{R_2}{R_1}}. \tag{7}$$

With the value of $R_{L,matched}$ determined, the complete circuit can be constructed. In is important to note that the value of $R_{L,matched}$ only applies for a particular distance between the coils. This is because the degree to which the coils are coupled, the mutual inductance M, decreases as the coil separation increases. Mutual inductance for circular coils is calculated from [1], [3]:

$$M = 2\mu_0 \frac{\sqrt{A+B}}{B}[(1 - \frac{\beta^2}{2})K(\beta) - E(\beta)] \tag{8}$$

where
$$A = \frac{a^2 + b^2 + D^2}{a^2 b^2}, \tag{9}$$
$$B = \frac{2}{ab}, \tag{10}$$
and
$$\beta = \sqrt{\frac{2b}{a+b}}. \tag{11}$$

In Equation (9), a is the radius of the transmitting coil, b is the radius of the receiving coil, and D is the separation distance between the two coils. The term $K(\beta)$ in Equation (8) is a first-order elliptic integral, and $E(\beta)$ is a second-order elliptic integral [1], [3]. The variable denoted μ_0 is the magnetic permeability of free space, $4\pi \times 10^{-7}$ H/m.

E. FERRITE MATERIAL

Ferrite is an iron-based material with important applications in electromagnetics. Transformer cores discussed previously are composed of ferrite because ferrite has a high magnetic permeability and a low electrical conductivity [11]. A low electrical conductivity is important because it reduces the probability that eddy currents will form within the material. According to Lenz's Law, the formation of eddy currents generate magnetic fields that oppose the field that created them [8]. Intuitively, this is undesirable considering the primary goal of IPT is to drive the magnetic flux toward a receiving coil.

Ferrite can be classified as either hard or soft. Hard ferrites are used to make magnets, while soft ferrites are used in electromagnetic applications involving inductance [15]. The ferrite used in this study is a soft Nickel-Zinc ferrite. In addition to being relatively inexpensive, ferrite is available off-the-shelf in a wide variety of dimensions and properties. For example, a flexible ferrite sheet with varying magnetic permeability can be obtained.

Magnetic permeability μ is an important factor for this analysis because it is the measure of a material's ability to support a magnetic field [16]. Magnetic permeability of a material is the product of the relative magnetic permeability μ_r times the permeability in a vacuum μ_0. In Chapter III, coils with ferrites of varying permeability are simulated, and it is shown that overall system efficiency is improved relative to coils in air alone.

In this chapter, prior research [1], [4], and [5] on the subject of WPT for AUVs was introduced briefly. The topic of ITP and its relation to mutually coupled coils was explained. Concepts such as compensating capacitance, mutual inductance, impedance matching, and magnetic permeability were discussed and related in order to set the stage for the construction of a series-series compensated circuit for use in testing and analysis. Finally, the derivation of the resistive load needed to match the impedance of the circuit was listed and explained. In the next chapter, a portion of the CST simulation results are presented along with a detailed explanation of the analogy used to arrive at the optimum ferrite configuration for the mutually coupled coils available for laboratory testing.

THIS PAGE INTENTIONALLY LEFT BLANK

III. CST SIMULATIONS

A. MODEL DESIGN

The purpose for using simulations with a numerical electromagnetics code (NEC) is to allow for the evaluation of many different models with various geometry and material configurations and properties. Compensating capacitance was also varied in order to demonstrate that efficiency suffers if conditions for resonance are not met. Despite the fact that over thirty different models were tested, less than one quarter of these were selected to be representative of the entire analysis.

CST Microwave Studio provides a platform for model construction that enables the user to manipulate numerous properties. The background material can be manipulated as well. For all simulated tests, the background was designated a vacuum with $\mu_r = 1$. It is important to note that as materials change, effectively changing the relative permeability, components remain visible but take on a different color. For example, the cores in Figure 9 are blue because this color represents a vacuum, while the back plates, which are composed of ferrite, are green. For the remainder of this chapter, this color scheme remains in effect. Of note, the color red represents seawater. Additionally, the circuit component colors have no significance.

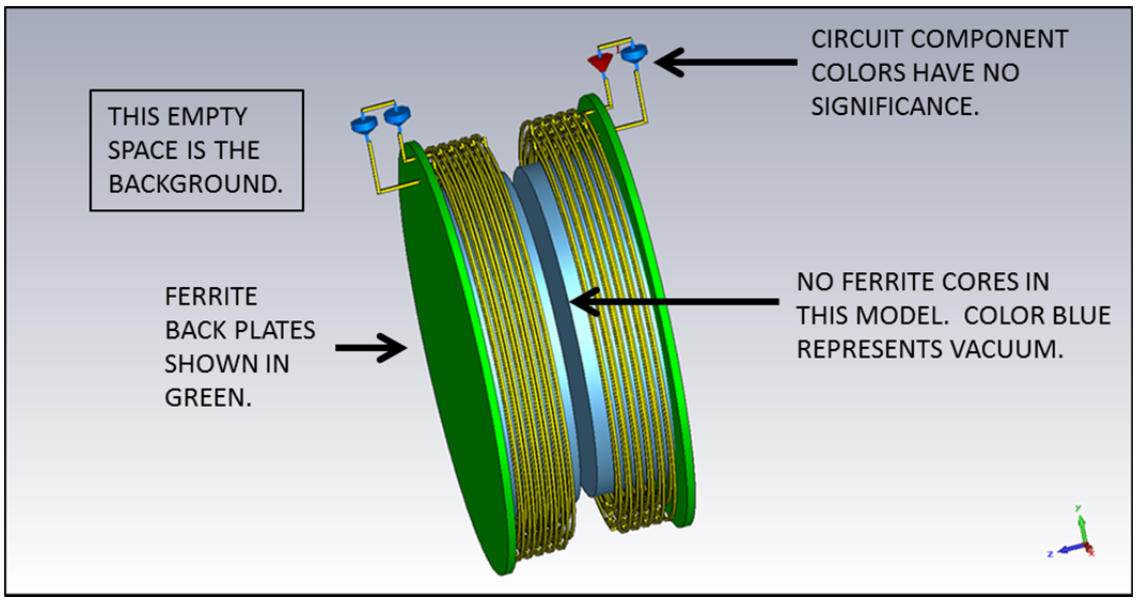

Figure 9. A two-coil model for simulation. The color blue represents vacuum, green is ferrite, and red is seawater. The circuit component colors have no significance.

The CST models were designed to simulate the actual coils used for laboratory testing as closely as possible. For this reason, the CST models had a coil radius of 60 millimeters and 20 coil turns. Parameters of the actual coils are listed in Table 1.

Table 1. Laboratory coil physical and electrical properties, from [1].

Coil Property	Transmitting Coil	Receiving Coil	Units
Coil Turns	20	20	turns
Coil Radius	60.325	60.325	millimeters
Coil Internal Resistance	0.23	0.21	ohms
Coil Impedance	83.35	83.33	microhenrys

The goal of using CST was to maximize the power-transfer efficiency over several parameters while operating in the frequency domain. The matched load depends on the mutual coupling, which is not known exactly; therefore, CST was used to perform a *parameter sweep* over a range of resistive load values from 20 Ω to 150 Ω. Once the simulations had concluded, the data was plotted on a polar plot (Figure 10) and the data

exported into a MATLAB script file that calculated efficiency for each resistive load value. The MATLAB script file is found in Appendix A.

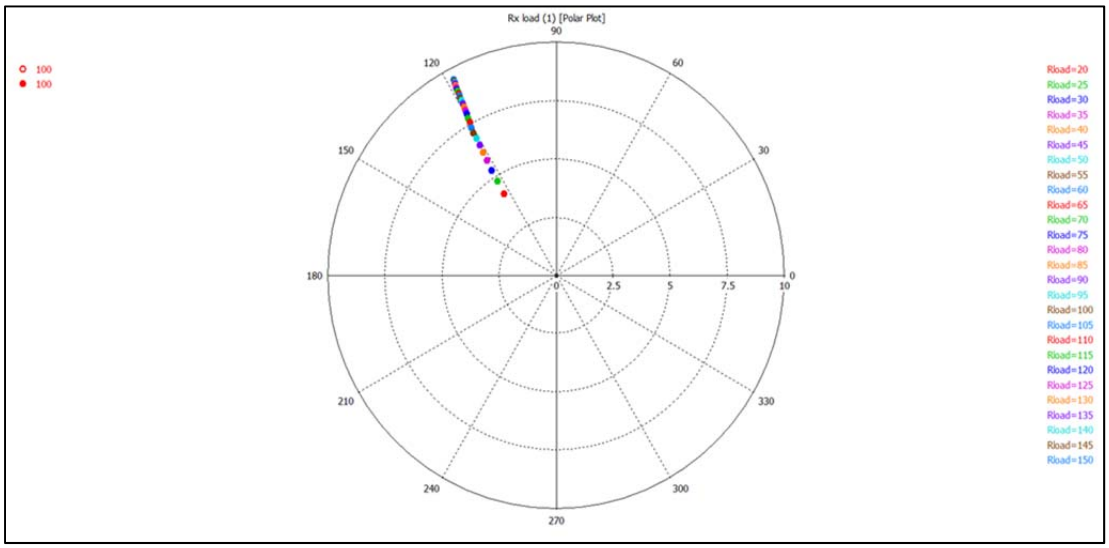

Figure 10. Example of a polar plot showing impedance values for a range of resistive loads.

B. SEPARATION DISTANCE CONSIDERATIONS

For the majority of CST simulations, the coil separation distance was maintained at 16.0 mm. A separation distance of this magnitude may seem arbitrary; however, this particular value was chosen with certain factors in mind. In particular, in prior research a separation of 16.0 mm was used due to coil mounting system constraints [1]. Specifically, the method used to secure the coils to the mounting stands during laboratory testing physically prevented moving the coils any closer than this (see Figure 11). Since the mounting system remained unchanged at the commencement of this study, 16.0 mm was used as the smallest distance in CST. After all simulations had been completed, the mounting system was redesigned and the limitation changed to 12.0 mm of separation due the protective polyethylene coating surrounding the coils (see Figure 12). Nonetheless, 16.0 mm remains applicable because it is likely that a production design of an AUV charging system would need to include a sheet of polymer-based material covering the charging unit to provide protection from sea pressure encountered at deep depths.

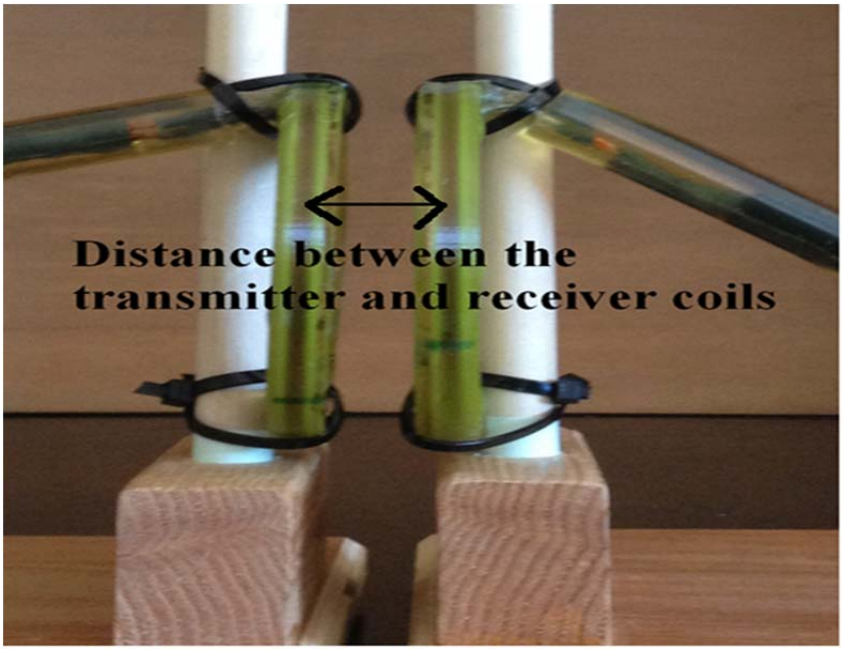

Figure 11. Distance between transmitting and receiving coils, coil mounting system used in prior research, and the zip ties that limit minimum separation distance, from [1].

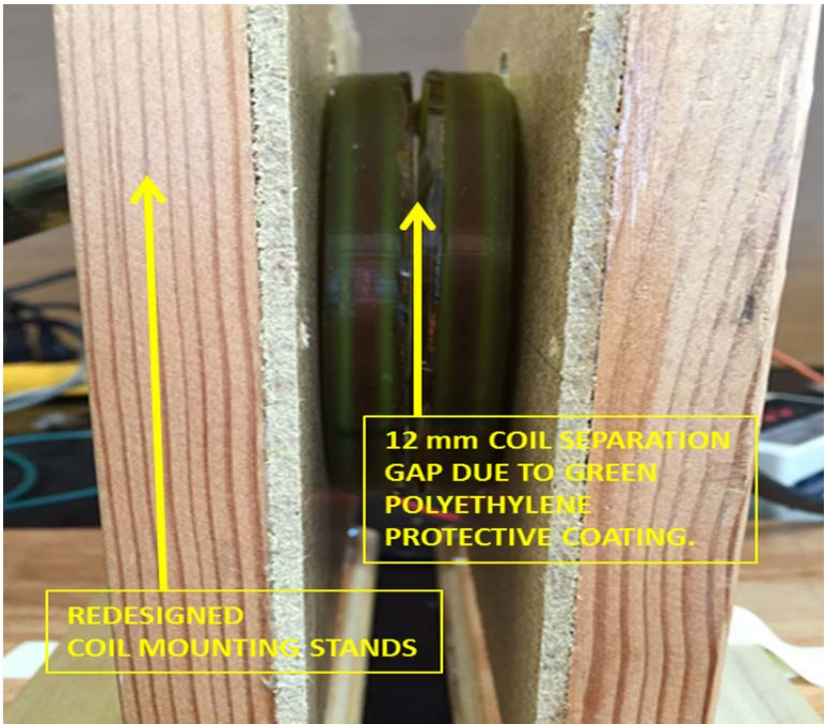

Figure 12. New coil mounting system which minimizes coil spacing.

A separation distance of 32.0 mm was used as the maximum distance for some of the simulation testing. This was done in consideration of the maneuvering capabilities of astern-powered AUVs that lack advanced bow thrusters or other multi-directional propulsion systems that are required to allow an AUV to hover with precision either over or under a charging system. Because of this, the AUV is required to lock itself into a charging system at a fixed distance, and 32.0 mm provides sufficient room to accomplish this.

C. SIMULATION RESULTS

The first model that was simulated consisted of the coils only (without the inclusion of ferrite) as seen in Figure 13. This was done to establish a baseline and because the actual coils were first tested in air during the laboratory-test phase of this study. A coil separation distance of 16.0 mm was selected. The model shown in Figure 13 is considered the reference model, and any parameter variations deviating from this model are highlighted in yellow in the results tables. The results for the reference model are provided in Table 2.

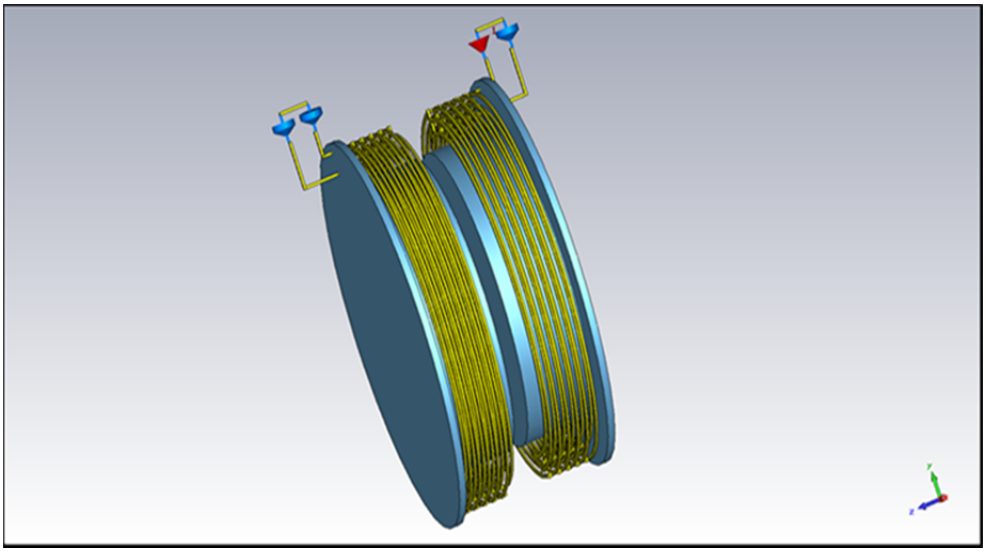

Figure 13. A CST model showing two mutually coupled coils in a vacuum.

Table 2. CST results for the reference model shown in Figure 13.

Model Type	Coils Only	Units
Ferrite Relative Magnetic Permeability	N/A	unitless
Width of Gap between Coils	16	mm
Ferrite Back Plate Thickness	N/A	mm
Ferrite Back Plate Radius	N/A	mm
Ferrite Core Wall Thickness	N/A	mm
Ferrite Core Depth	N/A	mm
Lateral Misalignment of Coils	0	mm
Compensating Capacitance	0	pF
Peak Efficiency	79.30%	unitless
Resistive Load at Peak Efficiency	50	Ω

The next model selected for simulation was designed with the inclusion of ferrite back plates with a relative permeability of 20. This permeability was selected to in order to maintain continuity with the prior study conducted in the laboratory [1] and to demonstrate how adding ferrite to the model, even with a relatively low permeability, still improves efficiency. The model is shown in Figure 14, and the results are shown in Table 3. The efficiencies are plotted against resistive load in Figure 15. For simplicity, all graphs use the following acronyms: Coils-only models are referred to as CO, coils with back plates are called CP, coils with solid cores and back plates are called CCP, and those with hollow cores are designated HCP.

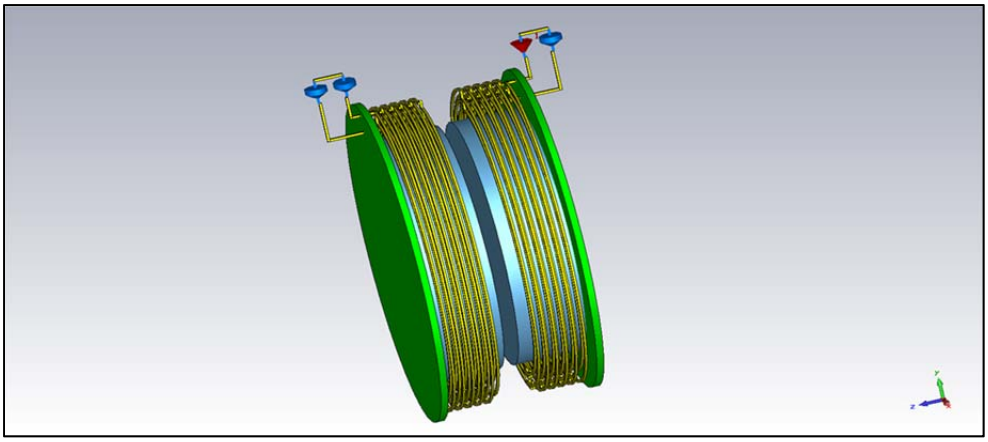

Figure 14. CST model showing ferrite back plates and a coil separation of 16.0 mm.

Table 3. CST results for the model shown in Figure 14.

Model Type	Coils with Back Plates	Units
Ferrite Relative Magnetic Permeability	20	unitless
Width of Gap between Coils	16	mm
Ferrite Back Plate Thickness	3	mm
Ferrite Back Plate Radius	72	mm
Ferrite Core Wall Thickness	N/A	mm
Ferrite Core Depth	N/A	mm
Lateral Misalignment of Coils	0	mm
Compensating Capacitance	0	pF
Peak Efficiency	83.10%	unitless
Resistive Load at Peak Efficiency	55	Ω

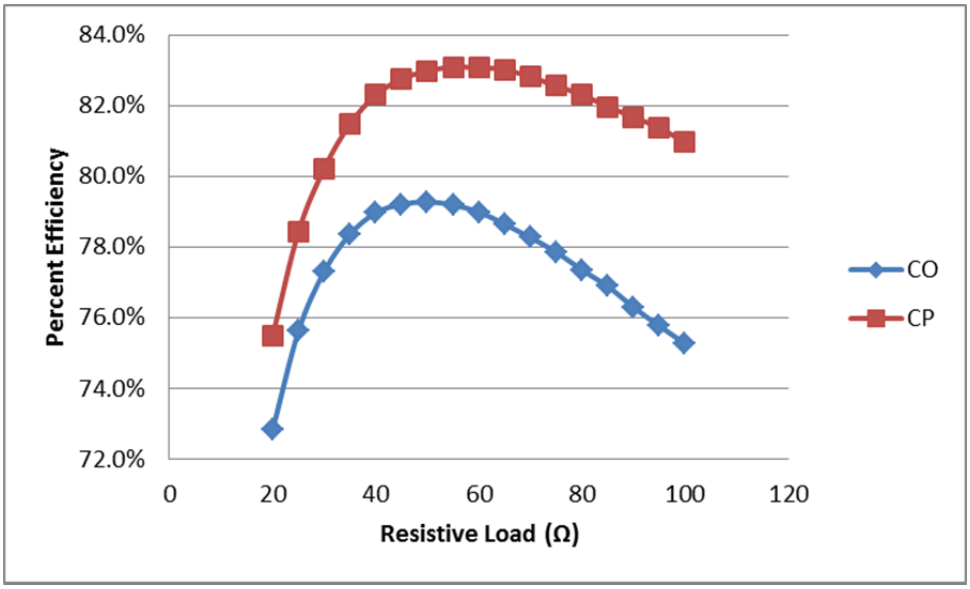

Figure 15. Efficiency comparison of CO and CP models.

Since there was a noticeable improvement in efficiency (83.1% vs. 79.3%) when back plates were added to the reference model, the next model simulation was designed using both back plates and solid ferrite cores. The idea for adding cores came from the knowledge that ideal, tightly-coupled transformers use an internal core to help concentrate the magnetic flux in the receiving coil. Despite a coil separation of 16.0 mm, adding cores allow the model to more closely simulate a tightly coupled system. The

model is shown in Figure 16, and the results are displayed in Table 4. In Figure 17, the comparison of efficiencies for CP and CCP models is shown.

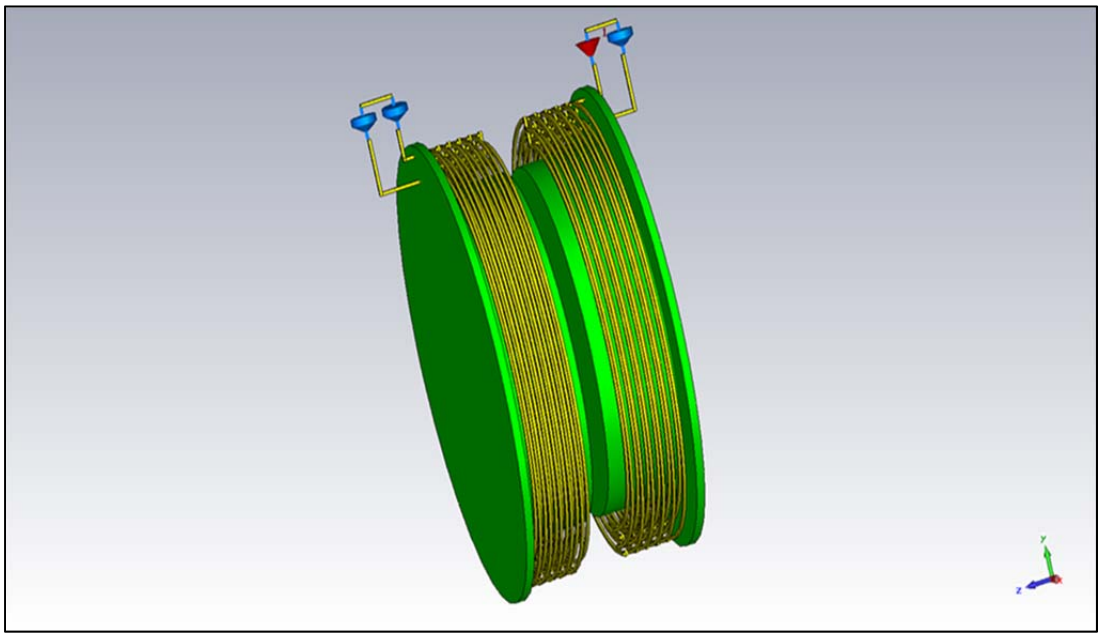

Figure 16. CST model with solid ferrite cores and ferrite back plates.

Table 4. CST results for the model shown in Figure 16.

Model Type	**Coils with Back Plates and Cores**	**Units**
Ferrite Relative Magnetic Permeability	20	unitless
Width of Gap between Coils	16	mm
Ferrite Back Plate Thickness	3	mm
Ferrite Back Plate Radius	72	mm
Ferrite Core Wall Thickness	Solid	N/A
Ferrite Core Depth	36	mm
Lateral Misalignment of Coils	0	mm
Compensating Capacitance	0	pF
Peak Efficiency	92.50%	unitless
Resistive Load at Peak Efficiency	110	Ω

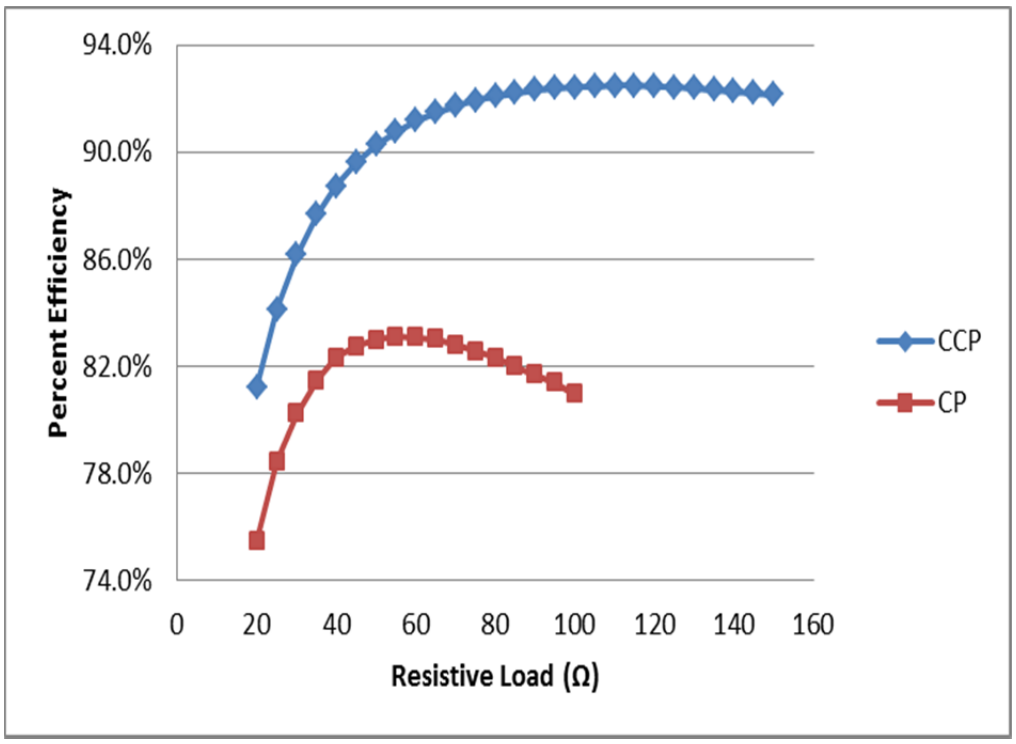

Figure 17. Efficiency comparison of CP and CCP models.

The addition of the ferrite cores caused a notable increase in peak efficiency (92.5% vs. 83.1%). The next step in the process of identifying an optimum model was to increase the relative magnetic permeability of the ferrite cores and back plates. The relative permeability of the ferrite simulated in CST ranged from 20 to 3000; however, the ferrite selected for laboratory tests and the remainder of CST simulations had a permeability of 220. This is because ferrite with permeability in excess of 220 did not show an increase in efficiency great enough to justify the excess cost. Models using ferrite with permeability of 220 did perform better than models using ferrites with permeability of 20 or 60. The results of the model constructed with ferrite back plates and cores with permeability of 220 are summarized in Table 5.

Table 5. CST results for model constructed with ferrite cores and back plates with relative permeability of 220.

Model Type	Coils with Back Plates and Cores	Units
Ferrite Relative Magnetic Permeability	220	unitless
Width of Gap between Coils	16	mm
Ferrite Back Plate Thickness	3	mm
Ferrite Back Plate Radius	72	mm
Ferrite Core Wall Thickness	Solid	N/A
Ferrite Core Depth	36	mm
Lateral Misalignment of Coils	0	mm
Compensating Capacitance	0	pF
Peak Efficiency	93.20%	unitless
Resistive Load at Peak Efficiency	120	Ω

With an ideal configuration of ferrite components now determined, the next step towards finding an ideal circuit was to determine the compensating capacitance that maximized power-transfer efficiency. A *parameter sweep* of capacitance was conducted using CST, and a MATLAB script file was used to identify which capacitance yielded the highest efficiency. The MATLAB script file is found in Appendix B. The results of the CCP model ($\mu_r = 220$) with compensating capacitance is summarized in Table 6, and a graph comparing the model with and without capacitance is shown in Figure 18.

Table 6. CST results for the CCP model ($\mu_r = 220$) with a compensating capacitance of 13.5 pF.

Model Type	Coils with Back Plates and Cores	Units
Ferrite Relative Magnetic Permeability	220	unitless
Width of Gap between Coils	16	mm
Ferrite Back Plate Thickness	3	mm
Ferrite Back Plate Radius	72	mm
Ferrite Core Wall Thickness	Solid	N/A
Ferrite Core Depth	36	mm
Lateral Misalignment of Coils	0	mm
Compensating Capacitance	13.5	pF
Peak Efficiency	96.80%	unitless
Resistive Load at Peak Efficiency	110	Ω

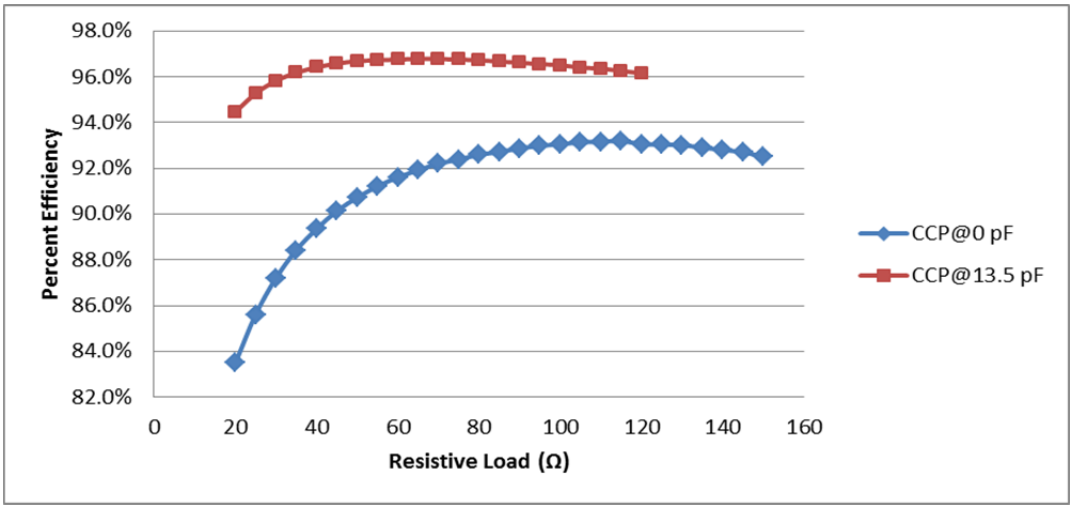

Figure 18. Efficiency comparison of the CCP model ($\mu_r = 220$) with and without capacitance.

After finding an ideal CST model that produced the highest efficiency, we next determined if replacing the solid ferrite cores with hollow versions adversely affected performance. If a model with hollow cores yields similar results, the cost and weight of the new charging system would be lower. More importantly, the overall weight of the new unit would not significantly affect the buoyancy characteristics of the AUV, particularly a small AUV like REMUS. The HCP model is shown in Figure 19. The results are shown in Table 7, and a graphical comparison of the CCP model ($\mu_r = 220$) and the HCP model ($\mu_r = 220$) is shown in Figure 20.

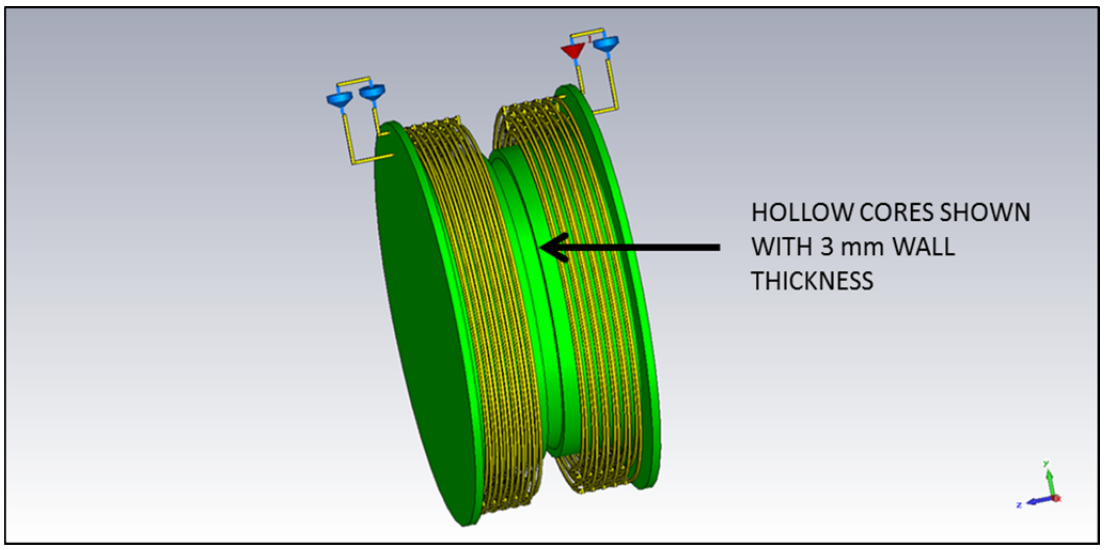

Figure 19. CST model showing hollow ferrite cores with wall thickness of 3.0 mm and ferrite back plates.

Table 7. CST results for model shown in Figure 19.

Model Type	Coils with Back Plates and Cores	Units
Ferrite Relative Magnetic Permeability	220	unitless
Width of Gap between Coils	16	mm
Ferrite Back Plate Thickness	3	mm
Ferrite Back Plate Radius	72	mm
Ferrite Core Wall Thickness	3	mm
Ferrite Core Wall Height	33	mm
Ferrite Core Depth	36	mm
Lateral Misalignment of Coils	0	mm
Compensating Capacitance	13.5	pF
Peak Efficiency	95.30%	unitless
Resistive Load at Peak Efficiency	95	Ω

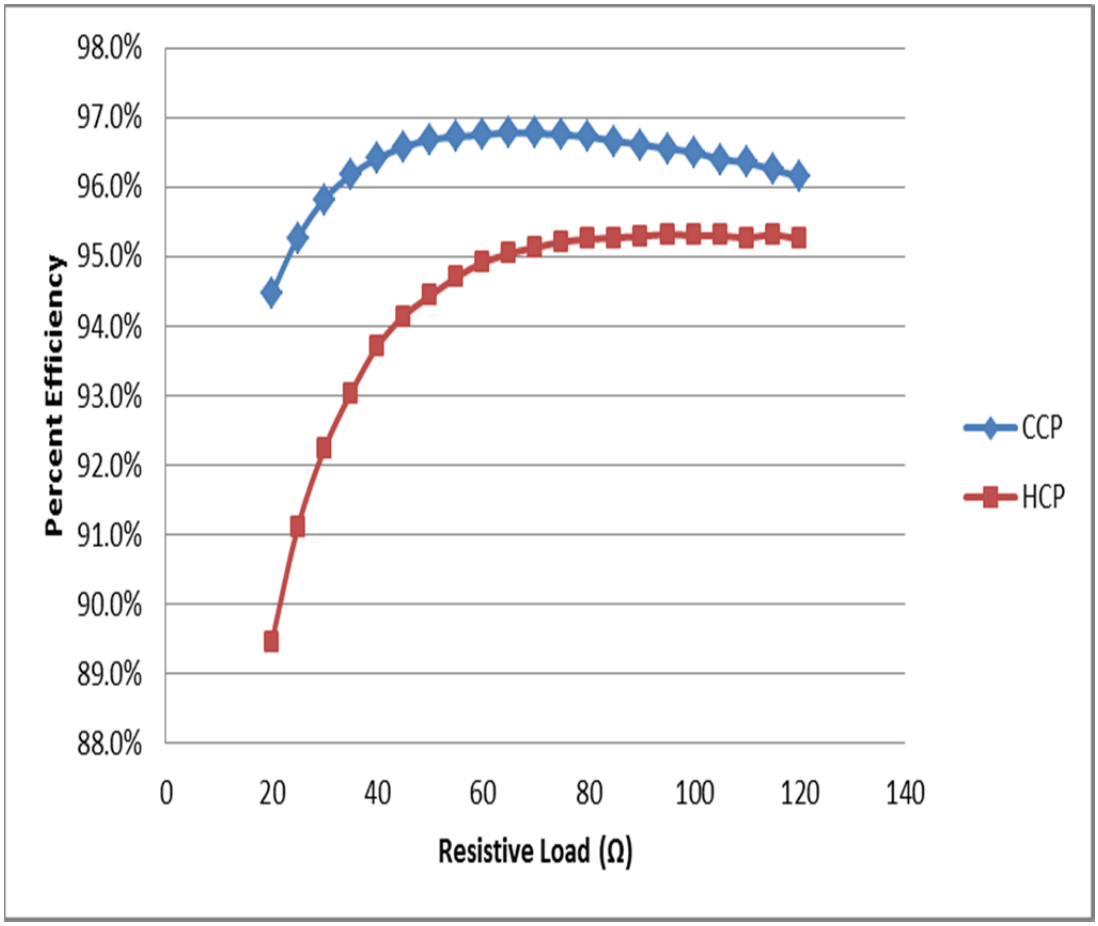

Figure 20. Comparison of CCP model (μ_r = 220) with the HCP model (μ_r = 220).

With a power-transfer efficiency close to the CCP model (95.3% vs. 96.6%), the HCP model proved a viable contender for a possible production model if cost and overall weight are considered a priority. The final step for CST simulation was to determine the power-transfer efficiency of a hollow core model with a core wall and back plate thickness of 0.1 mm. The objective was to accurately simulate a model that could be constructed in the lab. Ferrite with a thickness of 0.1 mm can be purchased in flexible sheets that allow the user to attach them to a variety of contoured surfaces. The CST model with 0.1 mm ferrite components is shown in Figure 21, and the results are shown in Table 8.

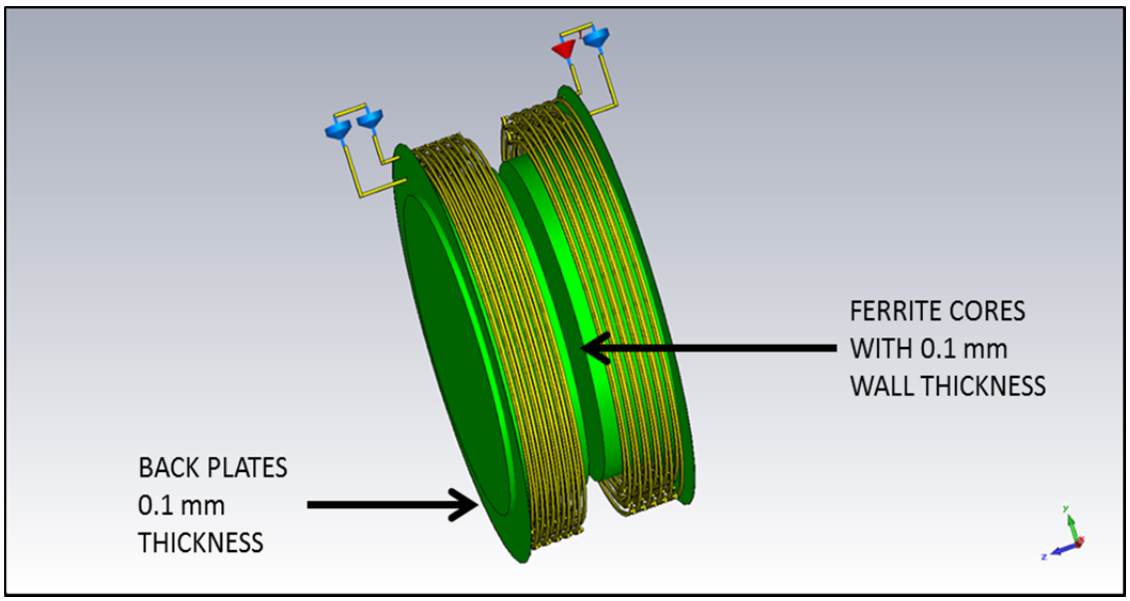

Figure 21. CST model showing hollow ferrite cores and back plates with a thickness of 0.1 mm.

Table 8. CST results for model shown in Figure 21.

Model Type	Coils with Back Plates and Cores	Units
Ferrite Relative Magnetic Permeability	220	unitless
Width of Gap between Coils	16	mm
Ferrite Back Plate Thickness	0.1	mm
Ferrite Back Plate Radius	72	mm
Ferrite Core Wall Thickness	0.1	mm
Ferrite Core Wall Height	33	mm
Ferrite Core Depth	33.1	mm
Lateral Misalignment of Coils	0	mm
Compensating Capacitance	13.5	pF
Peak Efficiency	86.70%	unitless
Resistive Load at Peak Efficiency	60	Ω

D. LATERAL MISALIGNMENT TESTING

In addition to considering coil separation distance for a production charging system design, lateral misalignment between the coils was investigated in order to provide meaningful data for designing an alignment system that would perform to

prescribed specifications. In other words, if it can be shown that misalignment of 5.0 mm, or even 10.0 mm does not cause a significant reduction in power-transfer efficiency, then an alignment system can more easily be designed with larger tolerances. A CST model with solid ferrite cores and back plates misaligned 10.0 mm off center is shown in Figure 22, and the results for 5.0 and 10.0 mm misalignments are shown in Table 9 and Table 10, respectively.

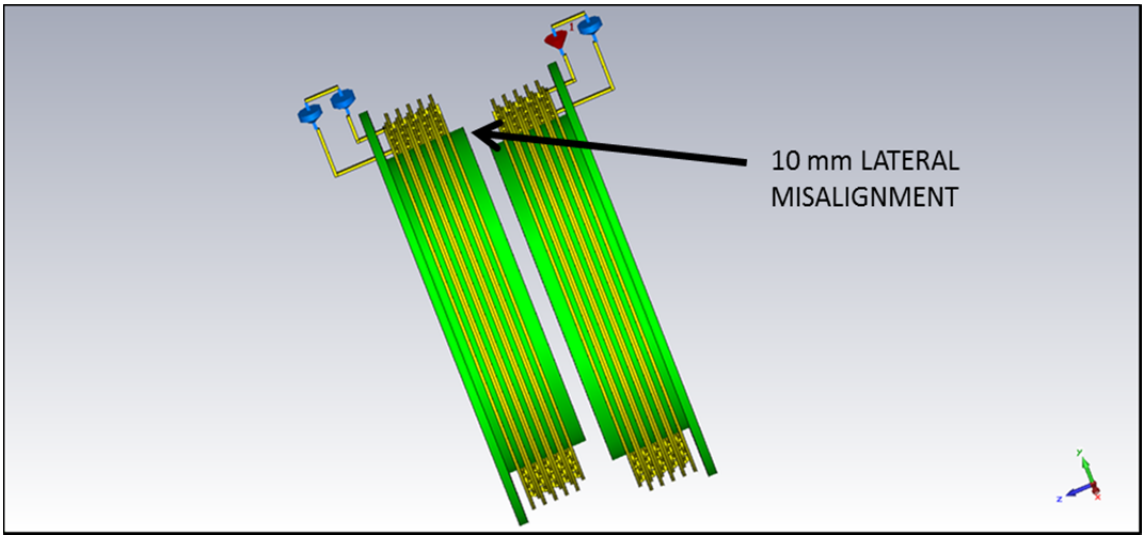

Figure 22. CCP model misaligned 10.0 mm.

Table 9. Results for CCP model misaligned 5.0 mm.

Model Type	**Coils with Back Plates and Cores**	**Units**
Ferrite Relative Magnetic Permeability	220	unitless
Width of Gap between Coils	16	mm
Ferrite Back Plate Thickness	3	mm
Ferrite Back Plate Radius	72	mm
Ferrite Core Wall Thickness	Solid	N/A
Ferrite Core Depth	36	mm
Lateral Misalignment of Coils	5	mm
Compensating Capacitance	13.5	pF
Peak Efficiency	96.70%	unitless
Resistive Load at Peak Efficiency	105	Ω

Table 10. Results for CCP model misaligned 10.0 mm.

Model Type	Coils with Back Plates and Cores	Units
Ferrite Relative Magnetic Permeability	220	unitless
Width of Gap between Coils	16	mm
Ferrite Back Plate Thickness	3	mm
Ferrite Back Plate Radius	72	mm
Ferrite Core Wall Thickness	Solid	N/A
Ferrite Core Depth	36	mm
Lateral Misalignment of Coils	10	mm
Compensating Capacitance	13.5	pF
Peak Efficiency	96.50%	unitless
Resistive Load at Peak Efficiency	105	Ω

According to simulation results, the reduction in overall power-transfer efficiency at 10.0 mm was negligible (96.5% vs. 96.8%). In terms of percentage, a 10.0 mm lateral shift over the entire 72.0 mm radius represents a factor of almost 14%. Having a misalignment of this magnitude yet still achieving acceptable power-transfer efficiency indicates adequate flexibility for the design of a new charging system for AUVs.

E. SENSITIVITY ANALYSIS

A sensitivity analysis was conducted in order to show that as the width of the gap increased, the CCP model (μ_r = 220) exhibited a much lower percent reduction in power-transfer efficiency compared to a model without ferrite. The results from the simulation confirm that a model loaded with ferrite continues to perform with an acceptable power-transfer efficiency as the coil separation distance increases. The results are shown in Table 11 and Table 12, respectively.

Table 11. Sensitivity analysis showing percent reduction in power-transfer efficiency from a 16.0 mm coil separation gap to a 32.0 mm gap for the CO model.

Model Type	Coils Only	Units
Ferrite Relative Magnetic Permeability	N/A	unitless
Ferrite Back Plate Thickness	N/A	mm
Ferrite Back Plate Radius	N/A	mm
Ferrite Core Type	N/A	mm
Peak Efficiency @ 16 mm	79.30%	unitless
Peak Efficiency @ 32 mm	54.60%	unitless
Percent Reduction in Efficiency	31.15%	unitless

Table 12. Sensitivity analysis showing percent reduction in power-transfer efficiency from a 16.0 mm coil separation gap to a 32.0 mm gap for the CCP model.

Model Type	Coils with Back Plates and Solid Cores	Units
Ferrite Relative Magnetic Permeability	220	unitless
Ferrite Back Plate Thickness	3	mm
Ferrite Back Plate Radius	72	mm
Ferrite Core Type	Solid	N/A
Peak Efficiency @ 16 mm	96.80%	unitless
Peak Efficiency @ 32 mm	90.22%	unitless
Percent Reduction in Efficiency	6.80%	unitless

The data clearly shows that the inclusion of ferrite in the models greatly reduces the sensitivity to changes in coil separation distance. This is perhaps the greatest advantage of adding ferrite. While an improvement of almost 17% efficiency between a model without ferrite and a CCP model at 16.0 mm is very promising, having a design that is not sensitive to a significant lateral misalignment and coil separation distance bodes well for the CCP model with respect to designing a practical charging system.

F. SEAWATER SIMULATION

It was desired to simulate the optimum model in a seawater environment for two important reasons. First, this produces results that closely resemble a mutually coupled coil system operating in an undersea environment. Second, physical testing of this configuration with seawater poses significant risks from an electrical safety standpoint if conducted in a laboratory setting. Seawater was simulated by placing a thin cylinder in the gap between the coils with a radius of 150.0 mm. The conductivity of the cylinder was set at 5.0 S/m to simulate this value. The relative permittivity ϵ_r was set to 80. In Figure 23, the seawater cylinder between the gap of the optimum model is shown. This is only an approximation to the actual scenario because of the limited volume of the seawater disk. Fewer magnetic field lines pass through the water disk than in the actual environment. A comparison of the efficiency reduction for the optimum model and the coils-only model is given in Table 13. Similar to the results seen when these two models are compared with respect to lateral separation, the optimum model displays a much lower reduction in efficiency. Plots of efficiency for the two models in seawater are shown in Figure 24.

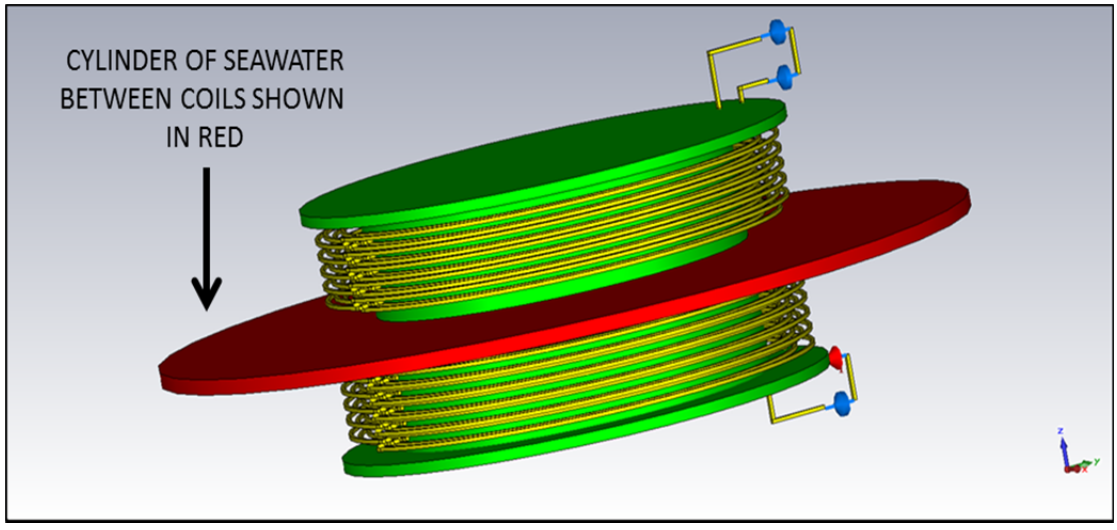

Figure 23. The CCP model is shown with a thin cylinder of seawater filling the 16.0 mm gap between the coils.

Table 13. Comparison of the efficiency reduction for a 16.0 mm coil separation distance when the CO model and the CCP model are moved from a vacuum to seawater.

	Vacuum	Seawater	Percent Reduction in Efficiency
Coils with Back Plates and Cores	96.8%	84.2%	13.0%
Coils Only	79.3%	43.3%	45.4%

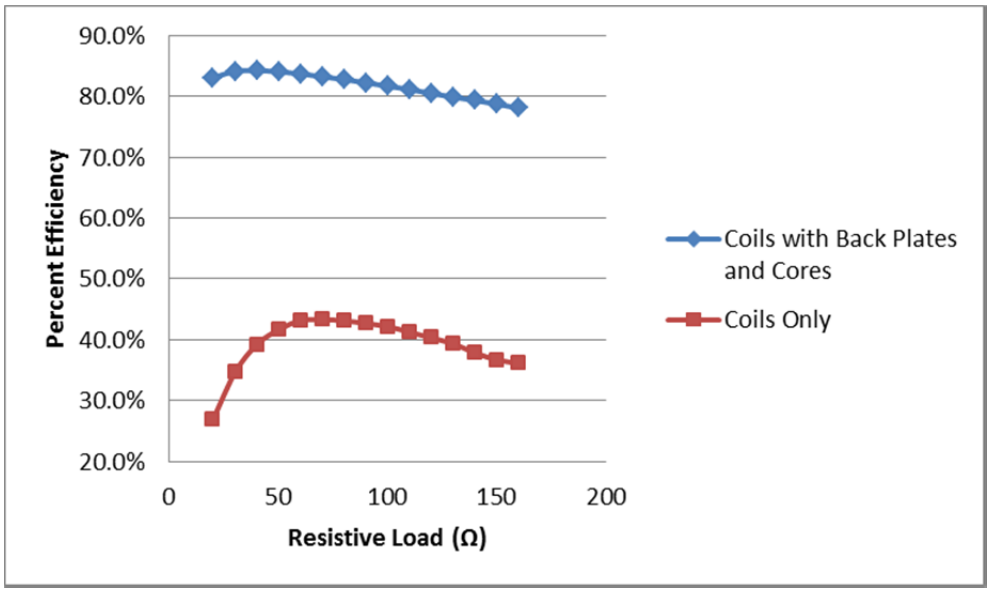

Figure 24. Efficiency comparison of optimum model and coils only model at 16.0 mm in seawater.

THIS PAGE INTENTIONALLY LEFT BLANK

IV. LABORATORY TESTING

A. SYSTEM SETUP

Having identified the optimum model that produced the highest power transfer efficiency through simulation, the next step in development was to verify the design with laboratory tests. The model selected for construction was a hybrid version of the optimum model, having a ferrite component thickness of only 0.1 mm to facilitate ease of construction. The circuit was constructed based on the series-series compensated circuit shown previously in Figure 8. A block diagram of the test setup is shown in Figure 25, and a photograph of the laboratory setup is shown in Figure 26.

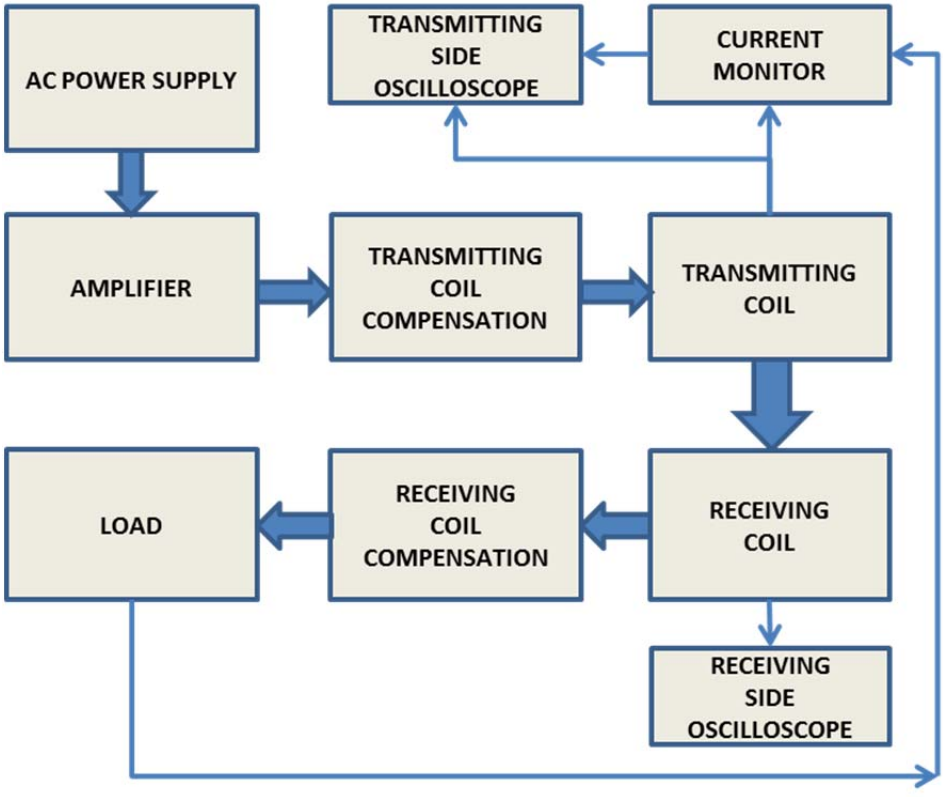

Figure 25. Block diagram showing components of laboratory test circuit.

For the transmitting side of the circuit, the power source was an Agilent 33220A function generator connected in series with an E&I 240L RF Power Amplifier. The

voltage on the transmitting side (Figure 26, point A) and current for both the transmitting side (Figure 26, point A) and the receiving side (Figure 26, point B) were monitored with a Tektronix TDS 3032B oscilloscope. On the receiving side of the circuit, voltage was monitored using a Tektronix TDS 2022B oscilloscope. The complete system setup is shown in Figure 26.

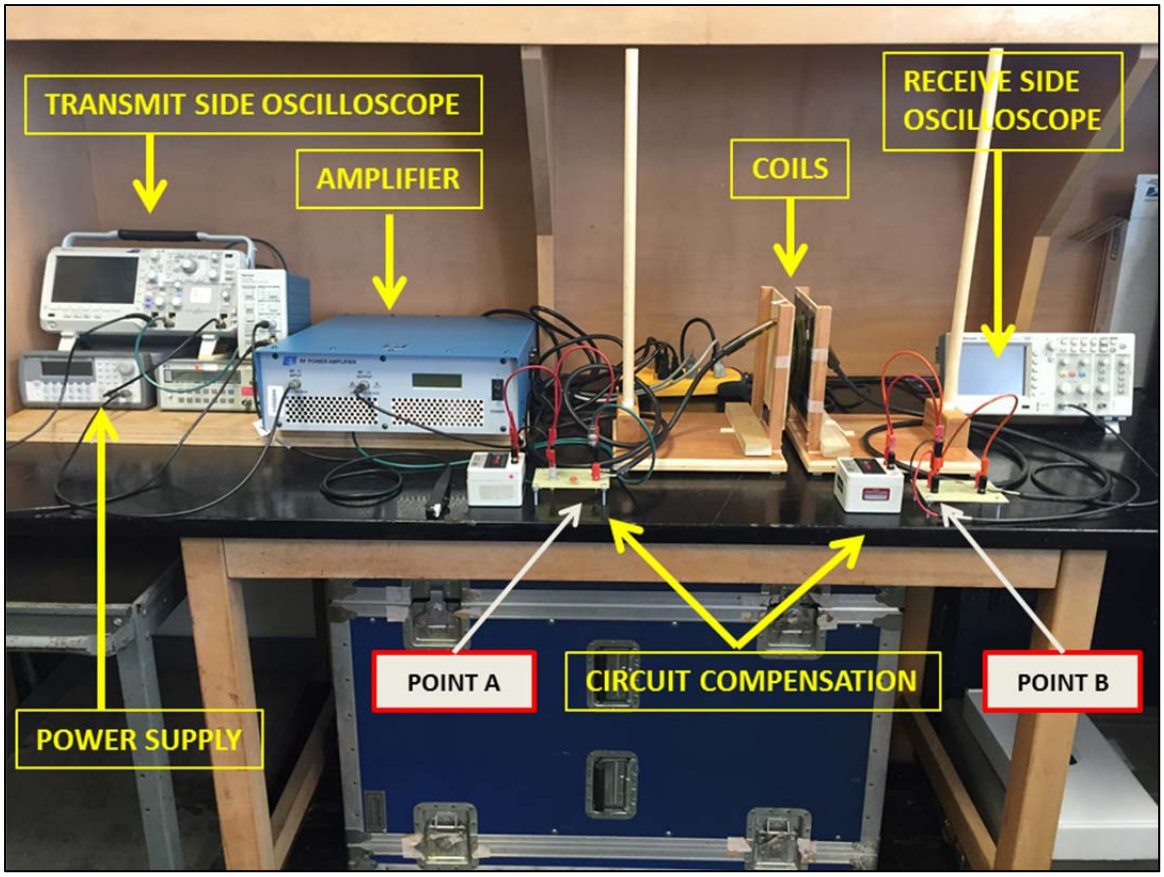

Figure 26. Laboratory setup displaying circuit components, power supply, and monitoring equipment.

Capacitance substituter boxes were initially considered for use as the compensating capacitors necessary for optimum circuit performance; however, these were ruled out due to inadequate operating limits, and instead fixed units were added with a capacitance of 15.0 pF (see Figure 27). Although CST simulation found 13.5 pF to be the optimum capacitance, further investigation with CST showed the difference in

efficiency to be negligible. A resistance substituter box with sufficient operating limits was used to select the appropriate resistive load for peak circuit performance.

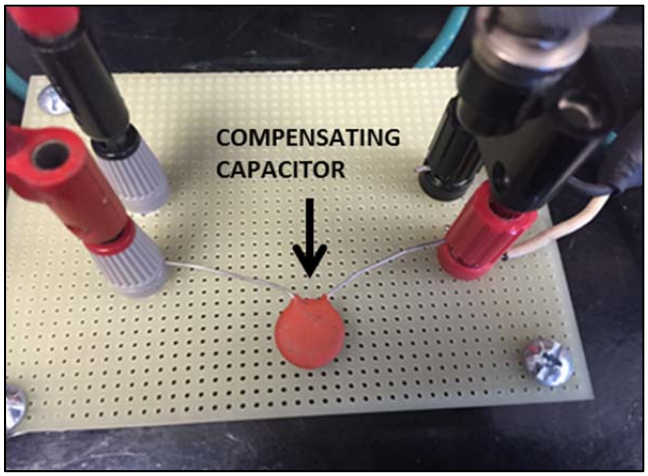

Figure 27. One of two 15.0 pF capacitors used to achieve optimum circuit performance.

The coils were placed on vertical wooden stands and attached using durable double-stick tape that facilitated easy removal of the coils for various tests (see Figure 28). The relatively large mounting surfaces of the stands compared to the size of the coils provided a favorable surface for ferrite placement. The height of the stand bases coupled with the large mounting surfaces provided the necessary elevation of the coils, which ensured any metallic constituents in the laboratory work bench did not electrically interfere with electromagnetic performance of the circuit. A photograph of one of the test coils mounted on its vertical wooden stand (without ferrite) is shown in Figure 29.

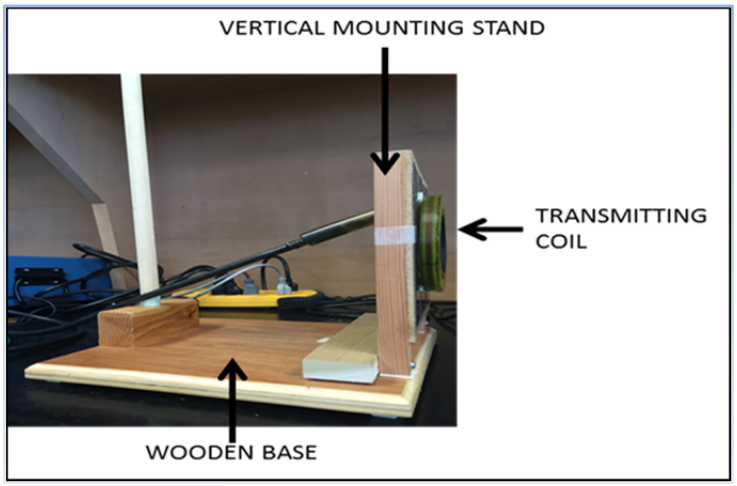

Figure 28. Transmitting coil mounted on vertical wooden stand and base.

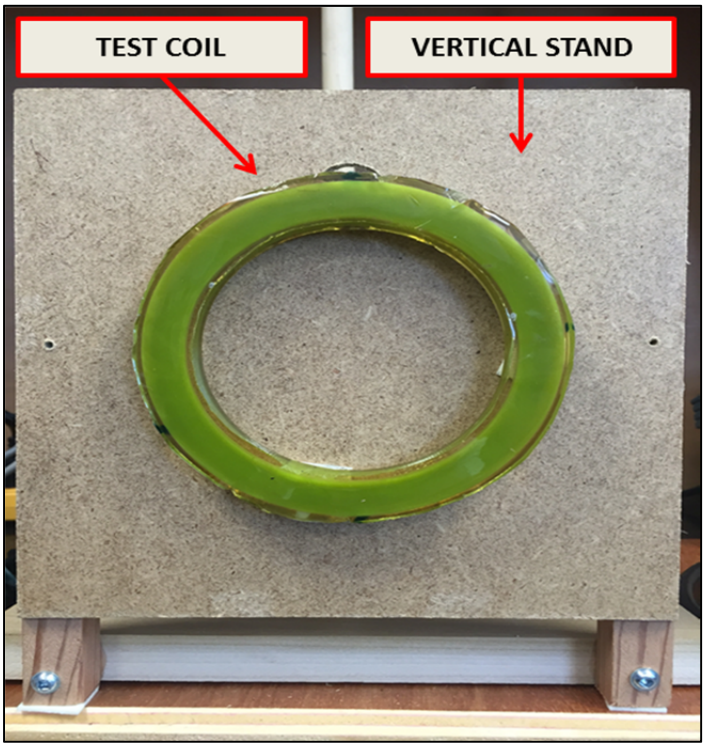

Figure 29. Test coil mounted on vertical wooden stand (without ferrite).

B. MEASURING POWER TRANSFER EFFICIENCY

Current was measured at the input to the transmitting coil and at the resistance substituter box of the receiving side of the circuit using a Tektronix TCPA 300 Amplifier and a TCP 305A current probe. Voltage was measured across both the transmitting and receiving coils. Using current, voltage, and the phase difference between the current and voltage waveforms, we computed the transmitted power as

$$P_t = V_{rms} I_{rms} \cos\theta. \tag{12}$$

In Equation (9), V_{rms} is the input rms voltage, I_{rms} is the input rms current, θ is the phase difference between the current and voltage waveforms, and P_t is the transmitted power. The power delivered to the resistance substituter box is

$$P_L = I_L V_L. \tag{13}$$

In Equation (10), V_L is the load voltage, I_L is the load current, and P_L is the power delivered to the load.

The data collected in the laboratory was the result of three distinct rounds of testing. In the first round, the coils were tested without ferrite. In the second round, ferrite sheets with a relative permeability of 220 were added behind the coils in order to mimic CST simulations conducted with ferrite back plates. This is shown in Figure 30. Finally, thin plastic cylinders covered with adhesive ferrite were placed inside the coils, while the ferrite behind the coils remained in place as shown in Figure 31.

For each round of testing, the coils were gradually moved apart in 4.0 mm increments beginning at 16.0 mm and ending at 32.0 mm. While 16.0 mm data was the primary focus in CST simulations, the laboratory tests were done at additional distances in order to establish the efficiency trend versus separation. The data is shown in Tables 14, 15, and 16, respectively. A graph comparing the efficiency versus coil separation distance for the three laboratory models is shown in Figure 32,

Figure 30. Test coil shown with ferrite back plate.

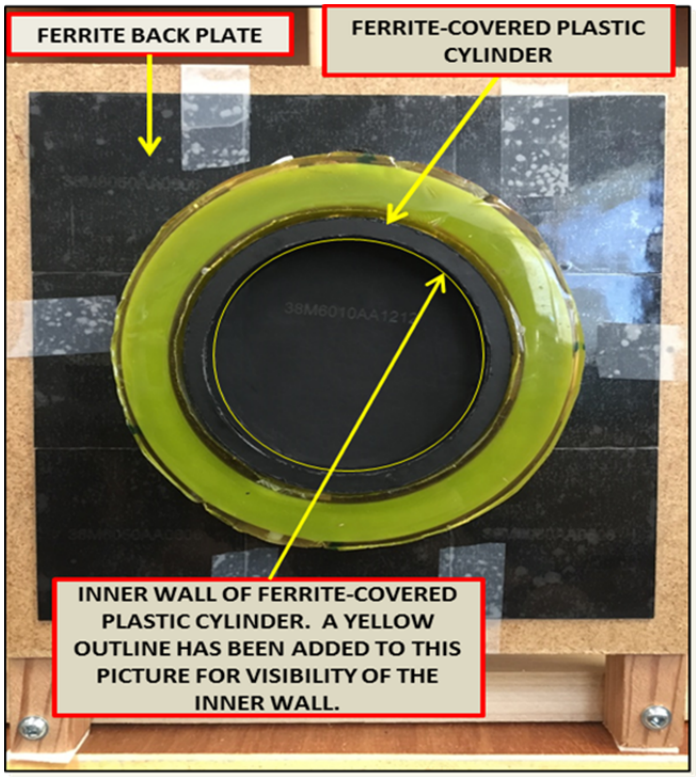

Figure 31. Test coil shown with ferrite back plate and ferrite-covered plastic cylinder.

Table 14. Efficiency results for round 1 (coils only).

V rms (V)	I rms (mW)	Load Voltage (V)	Load Current (mW)	Phase Angle (deg)	Coil Separation (mm)	Efficiency (%)
12.50	46.60	8.85	4.54	85	16	79.1%
12.50	46.60	7.82	3.98	85	20	61.3%
12.50	46.60	6.73	3.42	85	24	45.3%
12.50	46.60	5.85	2.97	85	28	34.2%
12.50	46.60	5.22	2.62	85	32	26.9%

Table 15. Efficiency results for round 2 (with ferrite back plates).

V rms	I rms	Load Voltage	Load Current	Phase Angle	Coil Separation (mm)	Efficiency
12.50	34.21	11.60	5.99	79.5	16	89.2%
12.50	34.21	10.51	5.42	79.5	20	73.1%
12.50	34.21	9.45	4.89	79.5	24	59.3%
12.50	34.21	8.55	4.34	79.5	28	47.6%
12.50	34.21	7.45	3.85	79.5	32	36.8%

Table 16. Efficiency results for round 3 (with ferrite back plates and hollow cores).

V rms	I rms	Load Voltage	Load Current	Phase Angle	Coil Separation (mm)	Efficiency
12.50	28.50	13.20	6.62	75.2	16	96.0%
12.50	28.50	12.11	6.31	75.2	20	84.0%
12.50	28.50	10.85	5.89	75.2	24	70.2%
12.50	28.50	9.75	5.12	75.2	28	54.9%
12.50	28.50	8.69	4.51	75.2	32	43.1%

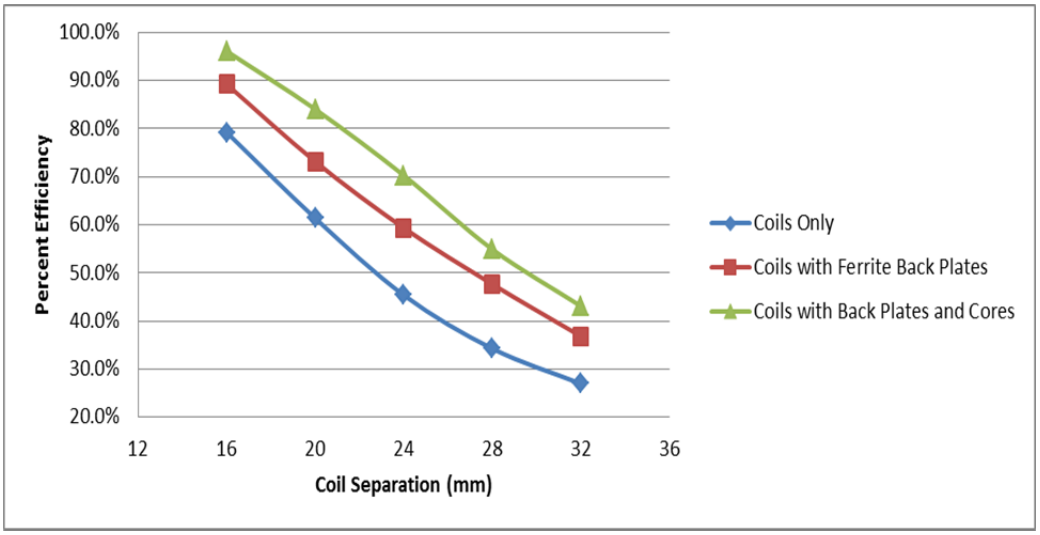

Figure 32. Efficiency of laboratory models for various coil separations.

The data clearly show that the addition of ferrite to the models results in an increase in power transfer efficiency. As such, it was expected that the laboratory version of the CST optimum model would exhibit only a minor reduction in efficiency as the lateral separation of the coils was increased in increments of 5.0 mm to a maximum separation of 10.0 mm. The results in Table 17 and Table 18 confirm this expectation.

Table 17. Lateral separation efficiency for coils with ferrite back plates and cores at 16.0 mm.

V rms	I rms	Load Voltage	Load Current	Phase Angle	Lateral Separation (mm)	Coil Separation (mm)	Efficiency
12.50	28.50	12.91	6.58	75.20	5	16	93.3%
12.50	28.50	12.54	6.47	75.20	10	16	89.2%

Table 18. Lateral separation efficiency for coils with ferrite back plates and cores at 32.0 mm.

V rms	I rms	Load Voltage	Load Current	Phase Angle	Lateral Separation (mm)	Coil Separation (mm)	Efficiency
12.50	28.50	8.32	4.29	75.2	5	32	39.2%
12.50	28.50	8.11	4.08	75.2	10	32	36.4%

C. COMPARISON OF SIMULATED AND MEASURED RESULTS

It is expected that computer simulation results are better than those attained in the laboratory. In a laboratory setting, realistic conditions coupled with various forms of error tend to reduce performance; however, this assumption is based on the expectation that the model or device itself closely represents the simulated version and vice versa. In the case of CST results versus laboratory model performance, the data are nearly the same for the coils without ferrite (79.1% vs. 79.3%). When ferrite is added, however, laboratory results are as much as 10% better than simulation results at 16.0 mm. The likely driver behind the efficiency difference lies in the configuration geometry of the ferrite back plate. Because the ferrite sheets are small squares, the square area of the laboratory back plate was almost 32% larger than the simulated circular back plate. When the area of the ferrite back plate was reduced to more closely match the CST model, the resulting efficiency was only 1.6% less than the efficiency determined by CST. The test coil with the reduced back plate is shown in Figure 33.

Figure 33. Reshaped ferrite back plate and test coil.

The trend seen with lateral separation efficiency reduction seems to contradict the previous data comparison but is actually easily explained by again referring to back plate

geometry. Recalling CST data from Chapter III, we found the reduction in efficiency for the optimum model at 10.0 mm was negligible (96.5% vs. 98.5%); however, at this same lateral separation in the laboratory, the efficiency reduction is much more pronounced (89.2% vs. 96%). This is because the same 10.0 mm shift results in a higher percentage of misaligned ferrite for a square back plate than it does for a circular one.

In Chapter I, it was mentioned that a study took place in 2013 [1] that provided the framework for this research. The same test setup and coils used then were initially used for this testing; however, the reported efficiencies in [1] were higher by 9%. Before the recent measurements were taken, however, an aging Krohn-Hite 50W Amplifier was replaced with the E&I 240L RF Power Amplifier. It was found that the old Krohn-Hite amplifier had some loose terminals, and the transmit circuit was not well matched to the amplifier. This caused a relatively large reflection that corrupted the voltage and current measurement at Point A in Figure 26. This is likely the source of the discrepancy between the two sets of data.

V. SUMMARY, CONCLUSIONS, AND FUTURE WORK

A. SUMMARY

In Chapter I, AUVs were introduced and their power systems were identified as a limiting characteristic of true autonomous operation. WPT, specifically IPT, was proposed as an alternative means of recharging onboard batteries, and REMUS was identified as the target AUV for this particular study. Seawater was mentioned as a severe hindrance to implementing this method, and ferrite was proposed as means boost the efficiency of an IPT system operating in this environment. A background for IPT, including the discussion of prior work [1], [4], and [5] in the field, was provided in Chapter II. In Chapter III, CST was used to identify the optimum ferrite configuration to maximize power-transfer efficiency. This model was then extensively simulated to show its viability as the optimum model. In Chapter IV, the IPT power circuit was constructed based on the theory discussed in Chapter II, and the model was built based on the results presented in Chapter III. This model then underwent extensive testing, and the measured results were compared to CST simulated results.

When comparing CST simulation and laboratory results, it is clear that they are very similar in terms of power-transfer efficiency. Even when laboratory testing the more complex model with ferrite back plates and cores, the results were close after the dimensions of the back plate more closely matched the model in CST. Because the seawater simulation only loosely approximated an actual undersea environment, further tests are required before an effort to replace present charging systems for AUVs (like REMUS) can go forward.

B. CONCLUSIONS

The objective of this research was to determine the optimum mutually coupled coil model to serve as the primary component of a replacement charger for the Navy's AUVs. Using CST simulations followed by laboratory testing, we showed that a specific geometric combination of ferrite in the vicinity of mutually coupled coils significantly improves power-transfer efficiency. Of equal importance is the data-supported indication

that the addition of ferrite makes the power system much less sensitive to changes in coil lateral misalignment and separation distance when compared to a model without ferrite. This allows more flexibility in implementation and operation of a WPT system.

While the objective of this research was met, this does not necessarily mean that an IPT charging system should replace all or even some of the systems currently in use. The decision to do so rests on the answer to the following question: Will the benefits of a complete system replacement outweigh the costs involved? For example, this decision should be made in favor of replacement if electrical shorts over an extended period of time created costs in excess of those associated with an overhaul. Likewise, replacement might be necessary or desired if a current system precluded the AUV from conducting operations that required more autonomy.

In any case, the technology, particularly in a seawater environment, requires more innovation before it can be considered a truly viable alternative. In the case of REMUS, for example, the test coils used in laboratory analyses were designed to fit inside the hull as shown in Figure 34. This is somewhat limiting because, as the size of the coil increases, it must be recessed further into the hull to prevent it from creating new hydrodynamic characteristics that require additional modifications to the AUV. As the coil is recessed, however, the internal electronics need to be altered or moved, again creating the need for additional modifications. From an electrical standpoint, there is an additional concern that the magnetic fields generated by the coils might potentially have an adverse effect on sensitive onboard electronics.

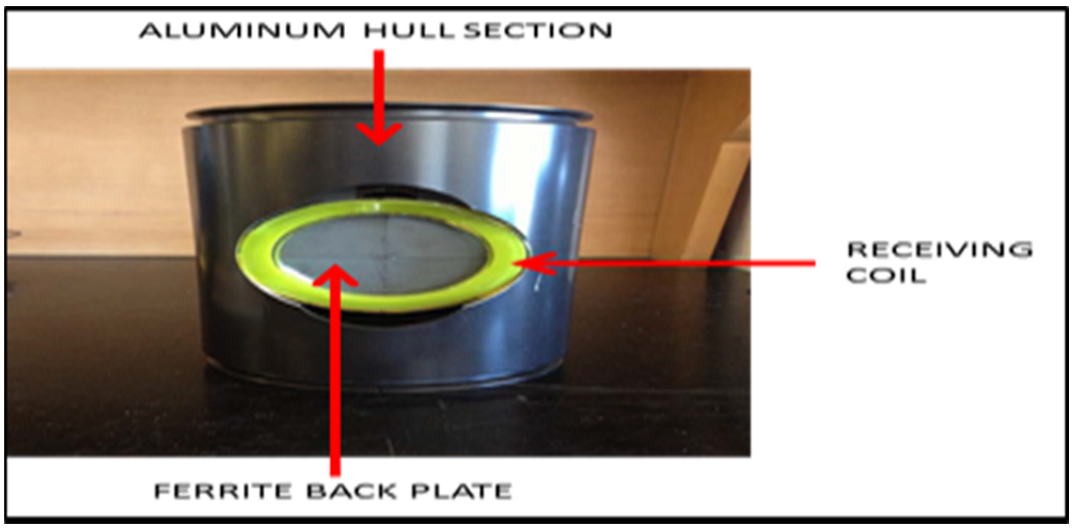

Figure 34. Test coil shown inside cross-section of aluminum representing REMUS hull, from [1].

C. FUTURE WORK

A possible solution to the problem of fitting the receiving coil inside the hull is to coil the wire around the circular hull itself. Since the length of most AUVs is larger than their diameter, the space available for adding additional turns is only limited by the length of the hull. Recalling the REMUS docking station displayed in Figure 1, we see that the transmitting coil could exhibit a similar design by having wire coiled around its circular geometry. Ferrite would still play a vital role in this design proposal. A large transmitting coil encapsulated in ferrite would be part of a charging station, and a smaller coil with ferrite backing would be wrapped around the AUV hull. Like REMUS and its docking station, the AUV with onboard receiving coil would drive into a larger transmitting coil that is part of the docking/charging station. The concept is illustrated in Figure 35.

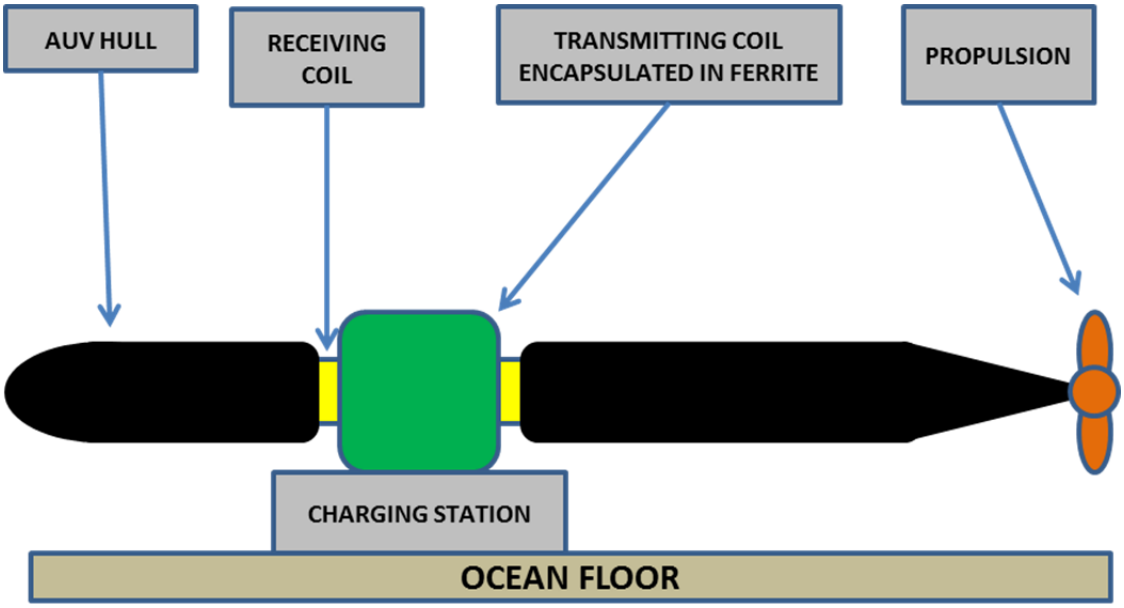

Figure 35. System mockup of AUV in docking/charging station.

Unmanned Aerial Vehicles (UAVs) could also benefit from battery charging by WPT. Specifically, UAVs can be remotely driven into a ground-based charging station, while small AUVs like REMUS need a more restraining system due to ocean currents. The fact that UAVs operate in air allows larger separation between the base station (transmit coil) and the client (receive coil) due to the ability to transmit power at higher frequencies in excess of the 100 kHz used in this research. Additionally, UAVs are utilized by the military and the civilian sector to a much greater extent than AUVs. This provides greater justification for incurring the cost of system replacement. A truly autonomous UAV charging system ensures maximum air-time for the completion of numerous missions.

APPENDIX A. MATLAB SCRIPT FILE: RESISTIVE LOADS

This appendix contains the MATLAB script file that inputs exported raw CST data and returns power-transfer efficiency for a parameter sweep of resistive loads.

```
% efficiency calculation from exported CST sweep data
% raw data file with comments is read

clear
clc

rad=pi/180;
pat1='='; pat2='/';

% read load voltage ------------------------------------------

fid=fopen('LV.txt');
% extract the parameter value from header (the number between = and /)
i=0;
linedat=0;

while feof(fid)==0
    linedat=fgetl(fid);
    P1=strfind(linedat,pat1);
    P2=strfind(linedat,pat2);
    p1=P1(1);
    p2=P2(1);
    S=linedat(p1+1);
    % convert the string characters to a number
    if p2-p1>1
        for n=p1+2:p2-1
            S=strcat(S,linedat(n));
        end
    end
    i=i+1;
    Rload(i)=str2double(S);
    linedat=fgetl(fid);
    % numerical entries
    linedat=fgetl(fid);
    D=sscanf(linedat,'%f');
    % D(1) is freq, D(2) is magnitude, D(3) is phase
    fkhz1=D(1);
    Vl(i)=D(2)*exp(j*D(3)*rad);
    linedat=fgetl(fid);   % blank line after each load
end

fclose(fid);
```

```
% read load current ----------------------------------------

fid=fopen('LC.txt');
% extract the parameter value from header (the number between = and /)
i=0;
linedat=0;

while feof(fid)==0
    linedat=fgetl(fid);
    P1=strfind(linedat,pat1);
    P2=strfind(linedat,pat2);
    p1=P1(1);
    p2=P2(1);
    S=linedat(p1+1);
    % convert the string characters to a number
    if p2-p1>1
        for n=p1+2:p2-1
            S=strcat(S,linedat(n));
        end
    end
    i=i+1;
    Rload(i)=str2double(S);
    linedat=fgetl(fid);
    % numerical entries
    linedat=fgetl(fid);
    D=sscanf(linedat,'%f');
    % D(1) is freq, D(2) is magnitude, D(3) is phase
    fkhz1=D(1);
    Il(i)=D(2)*exp(j*D(3)*rad);
    linedat=fgetl(fid);   % blank line after each load
end
fclose(fid);

% read load voltage ----------------------------------------

fid=fopen('PV.txt');
% extract the parameter value from header (the number between = and /)
i=0;
linedat=0;

while feof(fid)==0
    linedat=fgetl(fid);
    P1=strfind(linedat,pat1);
    P2=strfind(linedat,pat2);
    p1=P1(1);
    p2=P2(1);
    S=linedat(p1+1);
    % convert the string characters to a number
    if p2-p1>1
        for n=p1+2:p2-1
            S=strcat(S,linedat(n));
        end
```

```
    end
    i=i+1;
    Rload(i)=str2double(S);
    linedat=fgetl(fid);
    % numerical entries
    linedat=fgetl(fid);
    D=sscanf(linedat,'%f');
    % D(1) is freq, D(2) is magnitude, D(3) is phase
    fkhz1=D(1);
    Vi(i)=D(2)*exp(j*D(3)*rad);
    linedat=fgetl(fid);   % blank line after each load
end
fclose(fid);

% read load voltage ------------------------------------------

fid=fopen('PC.txt');
% extract the parameter value from header (the number between = and /)
i=0;
linedat=0;

while feof(fid)==0
    linedat=fgetl(fid);
    P1=strfind(linedat,pat1);
    P2=strfind(linedat,pat2);
    p1=P1(1);
    p2=P2(1);
    S=linedat(p1+1);
    % convert the string characters to a number
    if p2-p1>1
        for n=p1+2:p2-1
            S=strcat(S,linedat(n));
        end
    end
    i=i+1;
    Rload(i)=str2double(S);
    linedat=fgetl(fid);
    % numerical entries
    linedat=fgetl(fid);
    D=sscanf(linedat,'%f');
    % D(1) is freq, D(2) is magnitude, D(3) is phase
    fkhz1=D(1);
    Ii(i)=D(2)*exp(j*D(3)*rad);
    linedat=fgetl(fid);   % blank line after each load
end
fclose(fid);
disp(['number of blocks read: ',num2str(i)])
disp(['load values in order read: ',num2str(Rload)])
% compute efficiency
PF=angle(Vi./Ii);
Pin=abs(Vi).*abs(Ii).*cos(PF);
Pl=abs(Vl).^2./Rload;
Effic=Pl./Pin;
disp(['efficiencies: ',num2str(Effic)])
Effic'
```

THIS PAGE INTENTIONALLY LEFT BLANK

APPENDIX B. MATLAB SCRIPT FILE: CAPACITANCE

This appendix contains the MATLAB script file that inputs exported raw CST data and returns power-transfer efficiency for a parameter sweep of capacitance.

```
% efficiency calculation from exported CST sweep data
% raw data file with comments is read

clear
clc

rad=pi/180;
pat1='='; pat2='/';

% read load voltage ------------------------------------------

fid=fopen('LV.txt');
% extract the parameter value from header (the number between = and /)
i=0;
linedat=0;

while feof(fid)==0
    linedat=fgetl(fid);
    P1=strfind(linedat,pat1);
    P2=strfind(linedat,pat2);
    p1=P1(1);
    p2=P2(1);
    S=linedat(p1+1);
    % convert the string characters to a number
    if p2-p1>1
        for n=p1+2:p2-1
            S=strcat(S,linedat(n));
        end
    end
    i=i+1;
    Rload(i)=str2double(S);
    linedat=fgetl(fid);
    % numerical entries
    linedat=fgetl(fid);
    D=sscanf(linedat,'%f');
    % D(1) is freq, D(2) is magnitude, D(3) is phase
    fkhz1=D(1);
    Vl(i)=D(2)*exp(j*D(3)*rad);
    linedat=fgetl(fid);   % blank line after each load
end

fclose(fid);
```

```
% read load current ----------------------------------------

fid=fopen('LC.txt');
% extract the parameter value from header (the number between = and /)
i=0;
linedat=0;

while feof(fid)==0
    linedat=fgetl(fid);
    P1=strfind(linedat,pat1);
    P2=strfind(linedat,pat2);
    p1=P1(1);
    p2=P2(1);
    S=linedat(p1+1);
    % convert the string characters to a number
    if p2-p1>1
        for n=p1+2:p2-1
            S=strcat(S,linedat(n));
        end
    end
    i=i+1;
    Rload(i)=str2double(S);
    linedat=fgetl(fid);
    % numerical entries
    linedat=fgetl(fid);
    D=sscanf(linedat,'%f');
    % D(1) is freq, D(2) is magnitude, D(3) is phase
    fkhz1=D(1);
    Il(i)=D(2)*exp(j*D(3)*rad);
    linedat=fgetl(fid);   % blank line after each load
end

fclose(fid);

% read load voltage ----------------------------------------

fid=fopen('PV.txt');
% extract the parameter value from header (the number between = and /)
i=0;
linedat=0;

while feof(fid)==0
    linedat=fgetl(fid);
    P1=strfind(linedat,pat1);
    P2=strfind(linedat,pat2);
    p1=P1(1);
    p2=P2(1);
    S=linedat(p1+1);
    % convert the string characters to a number
    if p2-p1>1
        for n=p1+2:p2-1
            S=strcat(S,linedat(n));
        end
    end
```

```
    i=i+1;
    Rload(i)=str2double(S);
    linedat=fgetl(fid);
    % numerical entries
    linedat=fgetl(fid);
    D=sscanf(linedat,'%f');
    % D(1) is freq, D(2) is magnitude, D(3) is phase
    fkhz1=D(1);
    Vi(i)=D(2)*exp(j*D(3)*rad);
    linedat=fgetl(fid);   % blank line after each load
end

fclose(fid);

% read load voltage ------------------------------------------

fid=fopen('PC.txt');
% extract the parameter value from header (the number between = and /)
i=0;
linedat=0;

while feof(fid)==0
    linedat=fgetl(fid);
    P1=strfind(linedat,pat1);
    P2=strfind(linedat,pat2);
    p1=P1(1);
    p2=P2(1);
    S=linedat(p1+1);
    % convert the string characters to a number
    if p2-p1>1
        for n=p1+2:p2-1
            S=strcat(S,linedat(n));
        end
    end
    i=i+1;
    Rload(i)=str2double(S);
    linedat=fgetl(fid);
    % numerical entries
    linedat=fgetl(fid);
    D=sscanf(linedat,'%f');
    % D(1) is freq, D(2) is magnitude, D(3) is phase
    fkhz1=D(1);
    Ii(i)=D(2)*exp(j*D(3)*rad);
    linedat=fgetl(fid);   % blank line after each load
end
fclose(fid);
disp(['number of blocks read: ',num2str(i)])
disp(['load values in order read: ',num2str(Rload)])
% compute efficiency
PF=angle(Vi./Ii);
Pin=abs(Vi).*abs(Ii).*cos(PF);
Pl=abs(Vl).^2./95;
Effic=Pl./Pin;
disp(['efficiencies: ',num2str(Effic)])
Effic'
```

THIS PAGE INTENTIONALLY LEFT BLANK

LIST OF REFERENCES

[1] J. Cena, "Measuring power transfer efficiency of mutually coupled coils in an aluminum auv hull," M.S. thesis, Dept. Elect. Eng., Naval Postgraduate School, Monterey, CA, 2013.

[2] S. Kragelund and D. Homer. (2012, Nov. 15). AUV docking station integration with Monterey Inner Shelf Observatory. [Online]. Available: http://auvac.org/newsitems/view/1858

[3] V. Bana, G. Anderson, L. Xu, D. Rodriguez, A. Phillips, and J. Rockway, "Characterization of coupled coils in seawater for wireless power transfer," SPAWAR, San Diego, CA, Tech. Rep. 2026, 2013.

[4] T. McGinnis, C. Henze, and K. Conroy, "Inductive Power System for Autonomous Underwater Vehicles," *Oceans Vancouver BC*, vol. 112, no. 9, pp.1–5, Sept. 2007.

[5] B. D. Miller, "Design of an auv recharging system," M.S. thesis, Dept. Elect. Eng., Massachusetts Institute of Technology, Cambridge, MA, 2005.

[6] J. Muraoka. (2013, May 15). Off the chart robots underwater. [Online]. Available: https://prezi.com/mttp4eajflr-/underwater-robots/

[7] A. S. Mahajan and A. A. Rangwala, *Electricity and Magnetism*, Delhi, India: Tata McGraw-Hill, 1988, pp. 354–371.

[8] F. Ulaby, "Maxwell's equations for time-varying fields," in *Fundamentals of applied electromagnetics*, 5th ed., Upper Saddle River: Pearson Prentice Hall, 2007, ch. 6, pp. 255–270.

[9] Inductance and magnetic energy. (n.d.). web.mit.edu. [Online]. Available: http://web.mit.edu/viz/EM/visualizations/coursenotes/modules/guide11.pdf. Accessed Mar. 9, 2014.

[10] R. L. Myers, The Basics of Physics, Westport: Greenwood, 2006, pp. 264–271.

[11] U. A. Bakshi and M. V. Bakshi, *Transformers and Induction Machines*, Pune, India: Technical, 2008, pp. 15–32.

[12] C. P. Steinmetz, *Electric Discharges, Waves, and Impulses*, New York: McGraw-Hill, 1911, pp. 119–138.

[13] J. Fu, "Adaptive impedance matching circuits based on ferroelectric and semiconductor varators," Ph. D. dissertation, Dept. Elect. Eng., Univ. Michigan, Ann Arbor, MI, 2009.

[14] J. Garnica, J. Casanova, and L. Jenshan, "High efficiency midrange wireless power transfer system," in *IEEE MTT-S Int. Microwave Workshop Series on Innovative Wireless Power Transmission: Technologies, Systems, and Applications*, Kyoto, Japan, 2011, pp. 73–76.

[15] Z. Ullah, A. Shahid, and N. Shahzad, (2013, Apr. 5). Influence of pb doping on structural, electrical, and magnetic properties of sr-hexaferrites, *Journal of Alloys and Compounds*. *Volume 555*. [Online]. Available: http://www.sciencedirect.com/science/article/pii/S0925838812022852

[16] M. L. Kales, "Modes in wave guides containing ferrites," *Applied Physics*, vol. 24, no. 5, pp. 604–608, May 1953.

INITIAL DISTRIBUTION LIST

1. Defense Technical Information Center
   Ft. Belvoir, Virginia

2. Dudley Knox Library
   Naval Postgraduate School
   Monterey, California